THE LATE-TIME BOLOMETRIC LUMINOSITY OF SN 1987A

NICHOLAS B. SUNTZEFF, M. M. PHILLIPS, D. L. DEPOY, J. H. ELIAS, AND A. R. WALKER
Cerro Tololo Inter-American Observatory, National Optical Astronomy Observatories,[1] Casilla 603, La Serena, Chile
Received 11 November 1990; revised 2 January 1991

ABSTRACT

We present infrared photometry of SN 1987A in the *J*, *H*, *K*, *L*, *M*, 10, and 20 μm filters through day 1352 since the explosion of the supernova. We find that both the optical and mid-infrared magnitudes are slowly leveling out through day 1352 after their rapid decline in brightness during the epoch of dust formation. The near infrared colors ($V-J$, $V-H$, and $V-K$) initially reddened after dust formation around day 500, but by days 900–1000, they began to evolve to the blue, perhaps due to the thinning of the dust. Optical spectra obtained through day 1150 show no evidence for a sudden drop in the optical emission-line luminosities. This suggests that the region of optical emission has not undergone the so-called "infrared catastrophe," when the cooling of the ejecta becomes dominated by the infrared fine-structure lines, at least in the case described by the simple models of Fransson & Chevalier [ApJL, 322, L15 (1987)]. More complicated models where the higher density regions are cooled by the fine-structure lines at the same time that the nebular dust is thinning could be qualitatively consistent with the data. The infrared data have been combined with optical photoelectric and CCD *UBVRI* photometry obtained at CTIO to study the temporal evolution of the bolometric luminosity of SN 1987A. By day 1000, another source of energy beside the radioactive decay of ^{56}Co is needed to explain the slow leveling off to the bolometric luminosity decline. We can formally fit our data with the following energy sources: 5 ± 1 times the predicted ("solar") amount of ^{57}Co/^{56}Co; 10 ± 3 times the predicted amount of ^{44}Ti; or a constant energy input of 37.3 ± 0.15 dex [$\log_{10}$(ergs s^{-1})]. The energy input is unspecified; it could be a pulsar, light echo, or other unidentified energy source. Only the enhanced ^{57}Co/^{56}Co provides a good fit at all times to the data. The enhanced ^{57}Co, however, is in conflict with published hard x-ray and infrared spectral data. A careful reanalysis of the uncertainties in the observed hard x-ray and ultraviolet-optical-infrared fluxes, and the model predictions, suggests that *all* the data can be fit by the energy deposition from 0.075$\mathcal{M}_\odot$ of ^{56}Ni, a ^{57}Co/^{56}Co between 2.5 and 4 times "solar," and "solar" ^{44}Ti.

1. INTRODUCTION

The bolometric light curve of SN 1987A remains of fundamental interest more than a thousand days after the discovery of this important object in the Large Magellanic Cloud. It is perhaps the single most crucial observational tool available to us in attempting to understand the different energy sources which have powered the supernova during its evolution. It is now clear that the observed ultraviolet-optical-infrared ("uvoir") energy radiated by SN 1987A through day 900 has come from the exotic radioactive nuclides of ^{56}Ni and ^{56}Co (Hamuy *et al.* 1988; Suntzeff *et al.* 1988; Catchpole *et al.* 1988; Whitelock *et al.* 1988). Bolometric luminosity measurements made after day 550 have also provided important supporting evidence for the formation of dust in the supernova ejecta (Lucy *et al.* 1989; Suntzeff & Bouchet 1990, hereafter referred to as SB). More recently, the bolometric light curve has been cited as providing evidence for the presence of a pulsar in the supernova nebula (Bouchet *et al.* 1989b).

The amounts of these radioactive nuclides present after the supernova explosion give us clues as to the physical nature of the explosion. Since they are created in the extreme temperatures and densities that are reached in the few critical seconds of core collapse and explosion, they are direct products, in the same manner as the neutrinos, of a physical process that is poorly constrained by Earth-bound physical experiments.

To calculate the bolometric luminosity at any instant, it is necessary to sum the radiation emitted, from gamma rays to the far infrared, but to exclude any source, such as an echo, that is not directly part of the prompt energy release from the supernova and its ejecta. In practice, a natural division occurs between the high energy gamma rays and x rays, which can only be observed from satellite or balloon instruments, and the "uvoir" energy range, which is observable from ground-based telescopes. This division also has physical meaning, since the high-energy component effectively represents the energy emitted directly in the radioactive decays of newly synthesized nuclides, whereas the uvoir component is a measure of the thermalized energy derived from the same radioactive decays, or from other sources such as the initial shock wave produced by the explosion or a buried pulsar.

Since the discovery of SN 1987A, the staff of the Cerro Tololo Inter-American Observatory (CTIO) has carried out a systematic program of optical and infrared photometry, spectroscopy, and imaging observations, with one of the main objectives being the determination of the bolometric light curve. In a first paper dedicated to this topic, we combined our broadband *UBVRI* photometry data with infrared photometry obtained at the European Southern Observatory (ESO) to derive the evolution of the uvoir bolometric luminosity for days 1–903 (Suntzeff & Bouchet 1990). The main conclusion of this investigation was that, between days 126–903, the energy output of the supernova could be entirely explained by the radioactive decay of approximately 0.07$\mathcal{M}_\odot$ of ^{56}Co [assuming a distance modulus of 18.5 and a reddening $E(B-V) = 0.15$]. Evidence was also given for the formation of dust grains in the supernova ejecta, and an upper limit of 30% was derived for the contribution of an

[1] The National Optical Astronomy Observatories are operated by the Association of Universities for Research in Astronomy, Inc., under cooperative agreement with the National Science Foundation.

 0004-6256/91/031118-17$00.90

infrared echo to the far-infrared flux. In a second paper, spectrophotometric data obtained at CTIO, ESO, and the Kuiper Airborne Observatory were combined to independently derive the uvoir bolometric light curve between days 14–432 (Bouchet *et al.* 1991a). This method was shown to be more precise than determinations based on broadband photometry, but the conclusion was the same – i.e., $\sim 0.07 \mathcal{M}_\odot$ of ^{56}Co was produced in the explosion, and that the radioactive decay of this material was sufficient to explain the evolution of the uvoir bolometric luminosity from day 130 onwards.

Theoretical models predict that the decline rate of the bolometric light curve of SN 1987A should start to slow around day 1000 as ^{57}Co becomes the dominant radioactive species (Woosley 1988; Pinto *et al.* 1988; Kumagai *et al.* 1989; Woosley *et al.* 1989). Alternatively, the presence of a pulsar or accreting neutron star would also be expected to produce a flattening or slowing in the evolution of the bolometric luminosity (Woosley *et al.* 1989). In the present paper, we compare these predictions with measurements of the uvoir bolometric luminosity through day 1352 based on broadband *UBVRIJHK* imaging and 10 and 20 μm aperture photometry obtained at CTIO. In Sec. 2 we present the observations including selected low-resolution optical spectra, followed in Sec. 3 by a detailed discussion of the computation of the uvoir bolometric luminosity. The results are summarized in Sec. 4, and the evidence for energy sources in addition to ^{56}Co is critically examined.

2. OBSERVATIONS

2.1 Single-Channel Infrared Aperture Photometry

Single-channel infrared photometry is summarized in Table 1, which contains all CTIO data obtained after those published in Elias *et al.* (1988). The time in days listed in Table 1 is reckoned from the neutrino burst at JD 2446849.82 as observed by Bionta *et al.* (1987) and Hirata *et al.* (1987). All observations were made on either the 1.5 or 4 m telescopes at CTIO. The 10 and 20 μm data were taken with one of two gallium-doped germanium bolometers, one of which was also used to obtain the the shorter wavelength data on day 256. All the remaining data were taken with InSb photovoltaic diodes, mounted either in a dedicated Dewar or as an auxiliary photometric channel on the CTIO IR Spectrometer (Depoy *et al.* 1990). Data taken on the two systems are identical, except that the dedicated Dewar contained an L filter (effective wavelength = 3.45 μm) while the IR spectrometer contained an L' filter (effective wavelength = 3.75 μm). We will refer to these filters as the L(3.45 μm) or L(3.75 μm) filters. The passband of the L(3.75 μm) filter includes Brackett-α, while that of the L(3.45 μm) filter does not.

TABLE 1. Infrared photometry of SN 1987A.

	Observed Magnitudes[b]								
Day[a]	J	H	K	L	M	Ap.[c]	[10]	[20]	Ap.[d]
254	3.84	3.82	3.30	3.03	0.40(06)	22.8	0.48	...	12.7
256	...	...	3.28	3.02	0.60	12.7	0.56	-0.30(20)	12.7
257	3.86	3.84	3.32	2.50[e]	0.70	21x21	...	...	...
282	4.22	4.22	3.78	2.85[e]	0.97	3.5x7	...	...	...
284	4.27	4.27	3.86	3.59	0.94	6.2	...	...	...
285	4.26	4.26	3.84	3.56	0.89	9.3	0.86(05)	...	5.1
317	4.71	4.66	4.33	3.32[e]	1.38	10x21	...	...	...
318	4.73	4.64	4.34	3.32[e]	1.29	21x21	1.01	>-0.50[f]	12.7
321	4.76	4.71	4.38	4.07(08)	1.25	13.7	1.05(10)	...	12.7
347	5.06	4.96	4.74	3.62[e]	1.62	7x7	1.29	-0.15(10)	
377	...	...	...	...	...	...	1.51(08)	...	12.7
379	5.48	5.33	5.25	4.11[e]	2.08(06)	21x21	1.47(07)	...	12.7
433	6.18	5.87	6.04	4.80[e]	2.42	7x7	1.75	0.39(14)	5.1
468	6.55	6.21	6.57	5.57	2.80(06)	18.2	1.67(08)	...	12.7
648	9.40	9.04	9.62	7.83(19)	4.72(19)	12.7	1.56(10)	...	12.7
670	9.76	9.44	10.02	8.57(07)	5.19	6.2	2.04	-0.54(26)	4.3
935	...	...	...	...	...	...	5.65(11)	1.92(17)	4.3
1055[g]	...	...	...	...	...	...	6.73(18)	2.48(30)	4.3
1057	13.29	13.24	13.20	12.21(31)	>8.9[f]	6.2	...	...	...
1057	13.76	13.77	13.68	...	...	3.1	...	...	...
1115[g]	...	...	...	...	...	...	6.77(40)	>2.3[f]	4.3
1144[g]	...	...	...	...	...	...	7.57(21)	3.44(17)	4.3
1352[g]	...	...	...	...	...	...	7.99(26)	>4.1[f]	4.3

[a]Time in days after outburst, taken as JD 2446849.8 (see Suntzeff *et al.* 1989).
[b]Uncertainties are less than 5%, except as given in parentheses.
[c]Beam size in arcsec used for JHKLM measurements.
[d]Beam size in arcsec used for 10 and 20 μm measurements.
[e]'L' filter used instead of L filter for this measurement.
[f]Value given is 3σ upper limit.
[g]Data taken on 2 or 3 adjacent nights; date given is approximate mean date.

Uncertainties are indicated in the Table 1 when they are greater than 5%. Values below this level are predominantly limited by variations in transmission, and uncertainties in sensitivity and extinction corrections as determined from measurements of standard stars. Larger uncertainties are typically due to statistical uncertainties in the actual measurement of the supernova, with the exception of the measurements at 20 μm, where the best measurements (including all uncertainties) are no better than 10%.

The measurements after day 1000 deserve particular mention. As shown below, the *JHK* measurements of the supernova are seriously affected by surrounding nebulosity and companion stars; no correction for these effects has been made to the data in Table 1. For the days later than 1000, the 10 and 20 μm measurements are the average of measurements made over two day runs at the CTIO 4 m telescope (except the 20 μm measurement for day 1144, which only required one day). The total integration time was between 1 and 3 hr. Measurements were made in groups of 40 10 s pairs. Examination of the individual 40 pair groups and comparison of measurements made on adjacent nights shows no evidence for non-Gaussian errors. It should also be noted that the results were not biased by terminating the measurements at a given level of precision; rather, the available observing time was divided between the 10 and 20 μm observations based on a rough estimate of system efficiency and predicted signal.

2.2 Infrared Photometry from the CTIO Infrared Imager

We observed SN 1987A on days 1055, 1115, and 1351 at the $f/30$ focus of the CTIO 4 m telescope using the facility infrared imager. The imager employs a 58×62 InSb array and has a scale of 0.3 arcsecond pixel^{-1} for a field-of-view of $\sim 18''$. (See Fowler *et al.* 1987, for a more detailed description of the instrument.) Images were obtained through the broadband filters of J ($\lambda = 1.24$ μm; $\Delta\lambda = 0.30$ μm), H ($\lambda = 1.65$ μm; $\Delta\lambda = 0.27$ μm), and K ($\lambda = 2.20$ μm; $\Delta\lambda = 0.38$ μm). The supernova was observed several times through the filters at different positions on the array during each night. Equivalent measurements of the sky were interspersed among the observations of the object.

The data were reduced with the IRAF $V2.8$ reduction package.[2] The sky observations were combined with either a median filter or with the "maxreject" algorithm to form a

[2] IRAF is distributed by the National Optical Astronomy Observatories, which is operated by AURA, Inc., under contract to the NSF.

"star-free" sky image, which was then subtracted from the individual program frames. The sky-subtracted frames were flattened using sky flats, shifted, and added.

In Fig. 1 we present examples of the infrared images. We note two aspects of the supernova revealed in these images. The first is that there is a tremendous amount of extended near-infrared emission around SN 1987A that must be excluded when measuring the brightness of the supernova. The extended emission is most noticeable in J and H due to the lower sky noise, but is equally important in J, H, and K. The second aspect to note is that SN 1987A appears to be slightly extended in the H-band image from day 1255 towards position angle 100°. This elongation is similar in position angle and size of the ring seen in recent optical narrow band images of the supernova from the ESO New Technology Telescope (Gouiffes *et al.* 1989; see Fig. 3) and the *Hubble Space Telescope* (published in the popular media). There is no evidence for a coherent ringlike structure with a radius greater than 1.2″ that would indicate the presence of an infrared echo. The nebulosity, which is most prominently visible in the J-band image out to a radius of 3″ from SN 1987A, is wispy with no obvious symmetries.

The seeing was good during all the observations described above. For example, the full-width-half-maximum (FWHM) of SN 1987A in the 13 January 1990 H-band image is $\leqslant$0.6″ and was not well sampled by the 0.3″ imager pixels. In all cases the final, processed images were never worse than 0.75″ FWHM for days 1055 and 1144, and 1.1″ FWHM for day 1351.

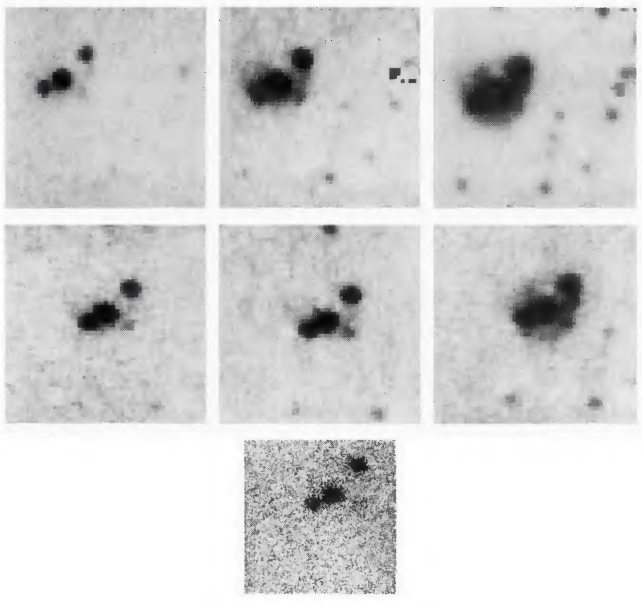

FIG. 1. Infrared images of SN 1987A on days 1055, 1115, and 1255 since outburst. The first row contains the *KHJ* images (left to right) from day 1055, and the second row shows the *KHJ* images from day 1115. The third row contains the H image from day 1255. In all the images, north is to the top and east is to the left. SN 1987A is the middle object in the obvious triplet of objects. Star 2 is at position angle 315° and 2.8″ from SN 1987A, while star 3 is at position angle 117° and 1.5″. The images in the first two rows are 17″ on a side. Note the tremendous amount of diffuse emission, especially in the J band, around SN 1987A. Note also the elongation of the H-band image of SN 1987A on day 1255 towards position angle 100°.

Aperture photometry was obtained from the calibrated images of the supernova, star 2, and star 3 in a synthesized 2″ diameter circular aperture. The sky was determined from the mode of the pixel values in an annulus 5.7″ to 8″ in diameter. Infrared standards from the list of Elias *et al.* (1982) were reduced to 2″ aperture magnitudes in the same way. Standards reproduce to $\pm$ 0.03 mag in the 2″ aperture. We tried using a smaller aperture size, but the results were less precise. The standards only agreed to $\pm$ 0.10 mag with a 1.2″ aperture, and the aperture corrections for a wider beam were uncomfortably large; the correction from a 2″ to an 8.8″ was $\sim$0.2 mag whereas the correction from 1″ was $\sim$0.4 mag. Point-spread-function fitting (Stetson 1987) was not attempted, due to the very small field of the imager and consequent lack of isolated stars to define the stellar profile.

The final InSb photometry for SN 1987A is listed in the first block of data in Table 2 along with the estimated errors (in parentheses) quoted in units of 0.01 mag. The actual errors returned by the aperture photometry program were on the order of 0.03 mag. Intercomparison of the two datasets and photometry from single frames, however, suggests that systematics conspire to cause an uncertainty in the measurement of $\sim$0.10 mag. We have also listed in Table 2 the averaged (for days 1055, 1115, and 1351) *JHK* photometry of star 2 based on the InSb imager data obtained at the 4 m telescope. Absolute photometry for star 3 based on InSb frames is not listed since star 3 is close enough to SN 1987A (1.6″) that even the 2″ aperture is contaminated by light from the supernova. Star 2 is far enough from the supernova (2.8″) that contamination from the light of the supernova was not a serious problem. Note that the colors for star 2 are very close to that of a mid-B to a mid-A star. This is consistent with the optical colors reported by Walker & Suntzeff (1990) where the observed $B - V$ color (uncorrected for reddening) was reported to be 0.06.

We include in Table 2 the magnitudes for SN 1987A measured for apertures of diameter 5, 6.3, and 7.5 arcsec, based on the imager data of days 1055 and 1115. These values were used to estimate the aperture corrections for the single-chan-

TABLE 2. CTIO infrared imager photometry.

Day	Object	J	H	K	Aperture Diameter (Arcseconds)	Notes
1055	SN 1987A	13.98(10)	13.83(10)	13.77(10)	2	1
1115		14.31(10)	14.38(10)	14.36(10)	2	1
1204		13.72(04)	13.43(06)	13.52(04)	6	1,2
1255		...	14.69(10)	...	1	3
1261		...	14.0 (10)	...	5	4
1351		15.17(10)	15.10(10)	15.06(10)	2	1
1055	SN 1987A	13.34(07)	13.34(07)	13.19(07)	5	1,5
1055		13.18(07)	13.19(07)	13.04(07)	6.3	
1055		13.11(07)	13.13(07)	12.96(07)	7.5	
1115	SN 1987A	13.62(07)	13.76(07)	13.68(07)	5	1,5
1115		13.43(07)	13.56(07)	13.50(07)	6.3	
1115		13.24(07)	13.47(07)	13.40(07)	7.5	
1255	SN 1987A	...	14.57	...	2	3
1255		...	14.24	...	3	
1255		...	13.91	...	4	
1255		...	13.71	...	5	
	Star 2	15.08(08)	15.09(08)	15.09(11)	2	6
	Star 3	...	15.19(06)	...	1	3,7
1055	Fuzz	14.7(3)	15.4(3)	14.7(3)	8.8	8
1115		15.2(3)	15.6(3)	15.4(3)	8.8	

NOTES: 1. InSb array at CTIO 4m. 2. Very poor seeing; observations taken at HA=6 hours. 3. PtSi array at CTIO 4m. 4. PtSi array at CTIO 0.9m. 5. Aperture centered on supernova. 6. Average of values taken on day 1055, 1115, and 1351 with InSb array at CTIO 4m. 7. Δ(H)(star 2- star 3)=-0.13±0.03. 8. Star 2,3, and SN 1987A subtracted from image.

nel detector measurements. For the correction from 2 to 5 arcsec, the flux in this annular region amounts to an equivalent magnitude of about 14.4 in *JHK*. Such a correction is 20% or more in *JHK* magnitudes taken through a 5″ aperture after day 900, and by day 1115, the flux in the supernova roughly equals the aperture correction. As can be seen in Fig. 1, both the 5″ aperture used at ESO and the 6.3″ aperture used at CTIO for single-channel photometry go right through star 2. Thus, the observed magnitude with a single-channel photometer can be strongly affected by both exact centering of the supernova in the aperture and the seeing. We have therefore chosen to ignore the CTIO single-channel values for day 1057 and use only the 2″ magnitudes from the imager data. Despite the caveats about centering and seeing, note in Tables 1 and 2 that the 6.3″ aperture photometry for days 1057 (single channel detector) and 1055 (infrared imager) agree quite well, to 0.16 magnitude or better.

We have included three other sets of imager measurements of SN 1987A in Table 2 in the first block of data. A set of InSb images in *JHK* were obtained on day 1204 at the CTIO 4 m telescope. The images were taken as SN 1987A crossed *under* the pole, and have very poor image quality. Magnitudes within a 6″ aperture are given. On day 1255, we obtained an excellent *H*-band image (0.6 arcsecond seeing) with the prototype CTIO Pt:Si imager at the 4 m. This image is presented in Fig. 1. Although the night was not photometric, the relative photometry through a 1 in. aperture is quite accurate. We have used the average *H* magnitude for star 2 (as listed in Table 2) to estimate the *H* magnitude for SN 1987A on this day. In addition, we find that $\Delta H(\text{star } 2 - \text{star } 3) = -0.13 \pm 0.03$. This *H*-band measurement of star 3 is included in Table 2. The *H*-band photometry through apertures of 2,3,4, and 5 arcsec centered on SN 1987A is included in Table 2. The final set of *H*-band images was taken on day 1261 with the prototype Pt:Si imager on the 0.9 m at CTIO. Because of the low quantum efficiency and small telescope aperture, this magnitude is of lower quality.

The final two entries in Table 2 (labeled fuzz) represents an attempt at measuring the strength of the extended emission. The "fuzz" is defined as the total flux in an 8.8 in. circular aperture centered in a 2 in. beam, with SN 1987A, star 2, and star 3 excluded. Star 3 was assumed to have the same $J - H$ and $H - K$ colors as star 2.

2.3 Optical Photometry

Aperture *UBVRI* photoelectric photometry for SN 1987A has been published by Hamuy *et al.* (1988), Suntzeff *et al.* (1988), and Hamuy & Suntzeff (1990). The latter paper summarizes all of the photoelectric observations made at CTIO of the supernova from day 3.8 to 813 since outburst. We have corrected the photoelectric photometry for the contamination by star 2, star 3 (these stars are identified in Fig. 1), and the faint nebulosity by subtracting (13.71,14.45,14.23,14.14,13.99) from the observed *UBVRI* aperture magnitudes, respectively. The amount of contamination was determined from the CCD data discussed in Walker & Suntzeff (1989) and represents the contamination in a 19 arcsec diameter aperture. To avoid large aperture corrections, we only used the corrected photoelectric data for days prior to 675. For *BVRI* the maximum aperture corrections were 0.08 mag. For *U*, the maximum correction was 0.14. The accuracy of the photoelectric photometry is 0.02 mag or better, as shown in Hamuy & Suntzeff (1990).

After day 675, we have used CCD photometry obtained at the CTIO 4 and 0.9 m telescopes. This data will appear in a forthcoming paper (Walker & Suntzeff 1991). We determined instrumental magnitudes for SN 1987A, star 2, star 3, and local standards within the CCD images with the DAOPHOT program (Stetson 1987) by fitting point-spread-functions determined from isolated stars on the frame to the overlapping images. The final standard magnitudes were determined using the local standard values given in Walker & Suntzeff (1990). We have estimated the internal photometric errors by fitting a running quadratic function to 12 data points around every data point and then calculating the dispersion of the observed data about the fit. The errors in *BVRI* for days 675 to 1000 are 0.035 magnitude or less. *U* during this period was accurate to 0.05 magnitude or better. From days 1000 to 1368, the errors increased to 0.03 in *BVR*, 0.04 in *I*, and 0.07 in *U*.

The photoelectric aperture magnitudes, corrected for contamination, and the CCD magnitudes agree to within a few hundredths of a magnitude at day 675, except for *I* where the CCD magnitudes are 0.27 magnitude brighter. This is reminiscent of the differences seen between the CTIO and SAAO photoelectric *I* magnitudes. Hamuy *et al.* (1988) concluded that this difference is due to the different filter/phototube responses for the CTIO and SAAO systems. Menzies (1989) later suggested that the CTIO *I* filter/phototube response was narrower in wavelength than the SAAO system. Hamuy *et al.* (1990) have since presented the actual *VRI* transmission curves which show that the CTIO *I* filter/phototube response is, indeed, narrower than that of the SAAO *I* filter. Both Menzies (1989) and Hamuy *et al.* (1990) showed that the difference in *I* magnitudes is entirely due to the different spectral regions being sampled by the two different *I* filters. Since the CTIO CCD *I* filter is an interference filter made to mimic the SAAO Cousins *I* filter/phototube transmission, the -0.27 jump between the photoelectric and CCD *I* magnitudes is also due to the different bandwidths of the *I* filters. We have left this jump in the data, since neither *I* magnitude is "more correct" than the other. This shift merely points out the dangers in using broad-band filters to sample a spectrum that is very different from the stellar spectra used to define the photometric system. Only in the plot of the photometric evolution of the *I* magnitude (see Fig. 2) and the $R - I$ and $V - I$ colors (see Figs. 3 and 4) have we corrected the photoelectric *I* magnitudes to the CCD *I* system by the shifts given by Hamuy *et al.* (1990).

2.4 Optical Spectrophotometry

Low-resolution optical spectrophotometry of SN 1987A obtained at CTIO through day 805 has been published by Phillips *et al.* (1988, 1990). These data are discussed in several papers (Blanco *et al.* 1987; Phillips 1988; Terndrup *et al.* 1988; Phillips & Heathcote 1989; Phillips & Williams 1990). The observations included in the present paper were obtained at a resolution of 11–16 Å (FWHM) using a GEC CCD detector on the Cassegrain spectrographs of the 1.5 and 4.0 m telescopes. Details concerning the acquisition and calibration of these spectra are given by Phillips *et al.* (1990).

3. COMPUTATION OF THE BOLOMETRIC LUMINOSITY

We performed the calculation of the "uvoir" (ultraviolet-optical-infrared) luminosity of SN 1987A following the pro-

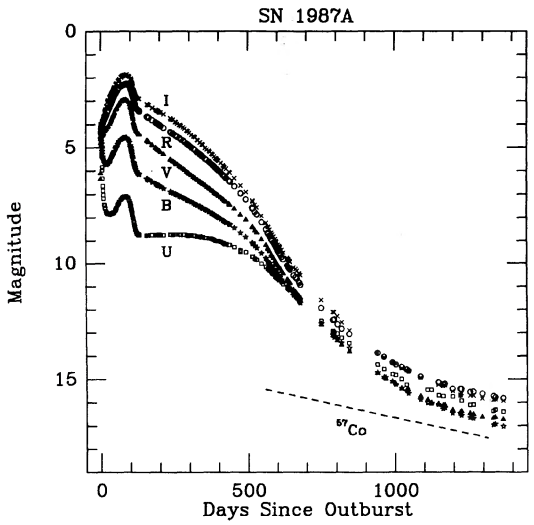

FIG. 2. Optical evolution of SN 1987A through day 1352. Around day 500, the supernova brightness began to decline very rapidly in all colors as dust began to form. By day 1000, the decline in brightness had slowed appreciably. The dotted line corresponds to the radioactive decay law of ^{57}Co, which is expected to dominate the energy input into the supernova nebular starting around day 1200.

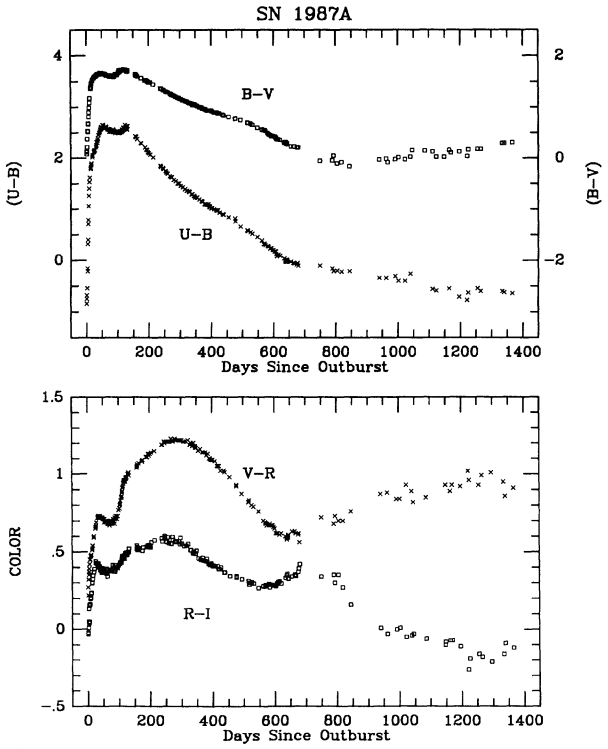

FIG. 3. Optical color evolution of SN 1987A. Note the sudden changes in color around day 600 at the time the dust formation. The evolution in all colors since the epoch of dust formation has been quite uniform. In the top panel the $U-B$ color is given on the left-hand ordinate and the $B-V$ color on the right-hand ordinate.

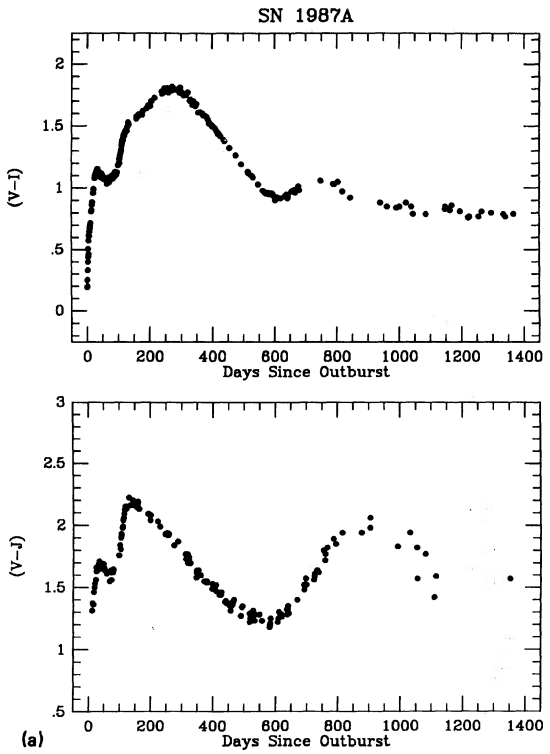

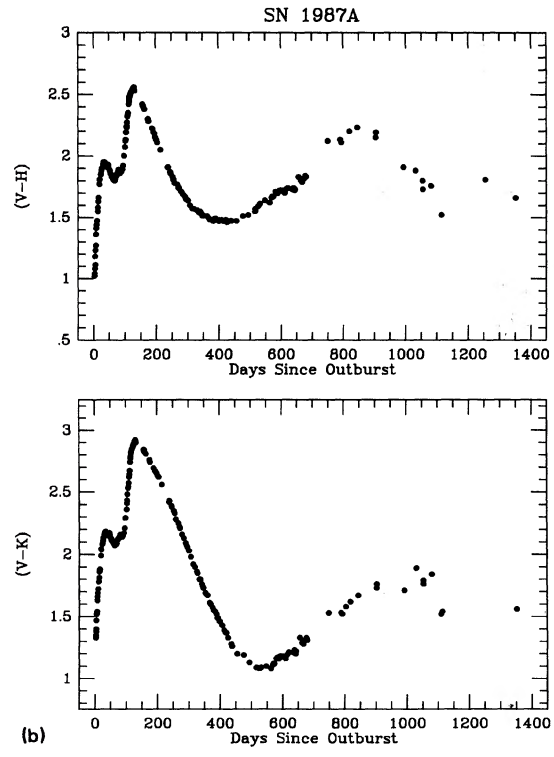

FIG. 4. Near infrared color evolution of SN 1987A. (a) shows the $V-I$ and $V-J$ evolution, and (b) the $V-H$ and $V-K$ evolution. Note the rapid reddening around day 500 in $V-J$, $V-H$, $V-K$ at the time of dust formation. $V-I$ shows a similar but much smaller, reddening around day 500. The $V-J$, $V-H$, and $V-K$ colors reverse their color evolution between days 800 and 1000, and begin to evolve towards the blue.

cedure discussed in SB. A true distance modulus of 18.5 and reddening of $E(B-V) = 0.15$ were assumed. Since one major step in the calculation, the extrapolation from the lowest frequency point (at 20 μm) to zero frequency, has been changed, we have recalculated the uvoir bolometric luminosity for the data discussed in SB. These data were a combination of CTIO optical photometry and ESO infrared photometry through day 903.

3.1 Preparation of the Data

For both the ESO/CTIO dataset (used in SB) and CTIO data set (Tables 1 and 2), we interpolated the optical and near-infrared data to the dates of the 10 and 20 μm observations. A quadratic fit to the 12 data points bracketing the date of observation gave an excellent fit to the temporal change in magnitude in all cases. We have left the discontinuity in the I magnitude at day 675 in the data. By this date, the 5 to 20 μm data completely dominated the flux distribution, and the effect of the discontinuity in I was smaller than the errors introduced into the calculation of the uvoir bolometric luminosity by the observational errors in the mid-infrared photometry.

For the ESO/CTIO data set, the ESO *JHKLM*, 10 μm, and 20 μm photometry was taken from Bouchet *et al.* (1989a) and Bouchet & Danziger (1991). The ESO *JHK* data have been corrected by Bouchet *et al.* (1991b) for an assumed contamination within the 5″ aperture of 14.7 in J and H, and 14.8 in K. We have compared the aperture magnitudes from the CTIO imager data taken on days 1055 and 1115 given in Table 2 with the corrected ESO photometry, and find that a further correction of 15.85 is needed to correct to the magnitude through the 2″ aperture. This procedure is the same as correcting the raw ESO *JHK* magnitudes for a contamination of 14.4 mag. We have also corrected the L and M magnitudes by 14.4, since the major sources of contamination are stars 2 and 3 which have colors similar to A0 stars.

We have filled in the gaps in the CTIO infrared data in Table 1 as follows. All gaps in *JHKLM* prior to day 379 were filled in by linear interpolation of the CTIO data. As shown in SB, for days before 400, since the 10 and 20 μm fluxes add at most 0.001 dex to the flux, these flux points can be ignored in the calculation. For day 935, we have interpolated the ESO *JHKLM* data to this date. We have shifted the ESO L (3.75 μm) and M data by 0.20 and -0.15, respectively, to bring the ESO magnitude scale onto the CTIO scale. This shift was determined by comparing observations [six for L (3.75 μm) and nine for M] taken close to the same dates.

The CTIO data after day 1000 were combined to form four distinct observations for the dates where 10 and 20 μm data were available (days 1055, 1115, 1144, and 1352). The 2″ aperture magnitudes in *JHK* from the CTIO InSb imager were used for days 1055, 1115, and 1352. We have the InSb imager data for days 1115 and 1351 to interpolate the *JHK* magnitudes to day 1144. The interpolated H magnitude for day 1144, based on Pt:Si data for day 1255 and the InSb data for day 1115, is the same as the magnitude based purely on the InSb imager data to better than 0.1 magnitude. We have adopted the ESO L(3.75 μm) and M magnitudes (shifted to the CTIO scale and corrected by 14.4 mag) for days 1057 and 1115. For days 1144 and 1352, we have estimated the L magnitude from the ESO L(3.75 μm) magnitudes (their last observation was on day 1316). For days 1144 and 1352, we have no information about the M magnitude, and have not included M in the basic photometric data. Finally, for day 1115, we have estimated the 20 μm magnitude by interpolating the CTIO 20 μm magnitudes to this date. The interpolated value is consistent with the upper limit on that date.

3.2 Calculation of the Bolometric Luminosity

As stated above, we have used the procedure outlined in SB to calculate the uvoir bolometric luminosity, with the following few changes:

We have adopted a simple linear interpolation between the flux points, as opposed to the logarithmic interpolation in SB. This has the effect of shifting the bolometric luminosity brighter by 0.02 dex (see Table 1 in SB). We have included the estimated photometric errors in the calculation to determine the error introduced by purely photometric errors. For the extrapolation from the longest wavelength flux point out to zero frequency, we have integrated the estimated scaled black-body distribution rather than assume a Rayleigh–Jeans law. Finally, we have attempted to calculate the error in the temperature and flux of the scaled blackbody, by estimating the most extreme values of these parameters via an interactive fitting procedure.

We have continued using the procedure discussed in SB of fitting an artificial point at 5.5 μm, based on a linear fit to the $K, L, N2, N3$, and $Q0$ magnitudes and including that point in the interpolation. This provides a rough correction for the CO emission. We have estimated the conversion factor from broad-band magnitude to monochromatic flux at the CTIO L(3.5 μm) magnitude by interpolating the K and L(3.75 μm) factors given by Bouchet *et al.* (1989a).

The estimated uvoir bolometric luminosity evolution of SN 1987A is given in Table 3 (CTIO data), and Tables 4 and 5 (ESO/CTIO data used in SB). In Table 3, we have included the following data: column (1) gives the number of days since explosion; column (2) gives the estimated bolometric uvoir luminosity for SN 1987A [in units of $\log_{10}$(ergs s^{-1}) based on the procedure given above]; column (3) lists the combined uncertainty in the bolometric luminosity due to photometric and fitting errors; column (4) gives the luminosity under the assumption that the flux from 20 μm out to zero frequency follows a Rayleigh–Jeans law; column (5) lists the estimated blackbody luminosity; column (6) lists the effective temperature of the scaled blackbody; column (7) lists the ratio of the flux in the blackbody longwards of 20 μm to the total luminosity in column 2; column (8) gives the infrared spectral index α (see SB); and column (9) gives the correction to the luminosity for CO emission. The luminosities quoted in columns 2 and 4 have been corrected for CO emission, except for days 1144 and 1352 where no correction has been applied since there was no M magnitude available.

In Table 4, we give the uvoir bolometric luminosity for the ESO/CTIO data for days 400 through 904. The column notation is the same as in Table 3. The differences between values in Table 3 and 4 are due to differences between the ESO and CTIO infrared measurements; the effects on the bolometric luminosity are no greater than 0.03 dex up to day 900.

In Table 5, we list the estimated uvoir bolometric luminosity for the ESO/CTIO data for days 14 through 378. These values were estimated from the dates where U to $Q0$ photometry was available. The differences between these data and the values published in SB are due entirely to the different

TABLE 3. Bolometric luminosity of SN 1987A from CTIO optical and infrared data.

Date (1)	$\log_{10}(L_{uvoir})$ (erg s^{-1}) (2)	$\sigma(\log_{10}(L_{uvoir}))$ (3)	$\log_{10}(L_{RJ})$ (erg s^{-1}) (4)	$\log_{10}(L_{BB})$ (erg s^{-1}) (5)	T_{eff} (K) (6)	$\frac{L_{BB}(>20\mu m)}{L_{uvoir}}$ (7)	α (8)	CO correction (9)
254	40.978	<0.02	40.978	...	...	0.00	0.3	-0.018
256	40.967	<0.02	40.968	...	...	0.00	0.4	-0.014
257	40.961	<0.02	40.961	...	...	0.00	0.4	-0.013
282	40.851	<0.02	40.852	39.75:	800:	0.00	0.2	-0.013
284	40.839	<0.02	40.840	39.80:	900:	0.00	0.1	-0.014
285	40.840	<0.02	40.840	39.80:	900:	0.00	0.1	-0.015
317	40.700	<0.02	40.700	39.70	800	0.00	-0.0	-0.012
318	40.697	<0.02	40.697	39.60	700	0.00	-0.0	-0.014
320	40.685	<0.02	40.685	39.60	700	0.00	-0.1	-0.016
347	40.573	<0.02	40.573	39.50	650	0.00	-0.1	-0.014
377	40.434	<0.02	40.434	39.35	600	0.01	-0.3	-0.012
379	40.428	<0.02	40.428	39.40	600	0.01	-0.3	-0.012
433	40.186	0.02	40.185	39.15	550	0.01	-0.5	-0.018
468	40.040	0.02	40.040	39.15	500	0.01	-0.9	-0.018
648	39.25	0.04	39.25	39.05	370	0.13	-2.5	-0.045
670	39.14	0.04	39.14	39.00	335	0.18	-2.7	-0.039
935	38.12	0.07	37.98	37.95	175	0.45	-2.8	-0.012
1055	37.91	0.10	37.70	37.80	155	0.58	-2.9	-0.006
1115	37.65	0.11	37.50	37.55	170	0.51	-2.9	-0.013
1144	37.59	0.12	37.37	37.45	150	0.56	-2.7	...
1352	37.12	0.21	36.88	37.00	180	0.49	-2.2	...

interpolation procedures adopted, since the extrapolation longwards of 20 μm does not affect the results given in Table 5. In column (1) we list the day; column (2) the estimated uvoir bolometric luminosity; and (3) the infrared spectral index.

3.3 Uncertainties in the Bolometric Luminosity

As discussed in Suntzeff *et al.* (1988) and SB, the major sources of error in the uvoir bolometric luminosity are the uncertainties in the distance modulus and reddening to SN

TABLE 4. Bolometric luminosity of SN 1987A from CTIO optical and ESO infrared data U to Q0 data.

Date (1)	$\log_{10}(L_{uvoir})$ (erg s^{-1}) (2)	$\sigma(\log_{10}(L_{uvoir}))$ (3)	$\log_{10}(L_{RJ})$ (erg s^{-1}) (4)	$\log_{10}(L_{BB})$ (erg s^{-1}) (5)	T_{eff} (K) (6)	$\frac{L_{BB}(>20\mu m)}{L_{uvoir}}$ (7)	α (8)
399.7	40.351	<0.02	40.352	39.28	600	0.01	-0.4
455.7	40.100	<0.02	40.101	39.17	550	0.01	-0.7
518.1	39.803	0.02	39.803	39.09	500	0.02	-1.1
526.1	39.761	0.02	39.760	39.10	500	0.02	-1.2
616.0	39.346	0.03	39.350	39.11	385	0.11	-2.3
636.0	39.273	0.03	39.283	39.08	370	0.13	-2.5
641.0	39.231	0.03	39.229	39.01	370	0.12	-2.4
670.0	39.167	0.04	39.189	38.92	290	0.18	-2.8
692.0	39.048	0.04	39.017	38.90	270	0.26	-2.8
698.0	38.965	0.04	38.953	38.73	270	0.21	-2.7
734.0	38.871	0.05	38.891	38.65	250	0.25	-3.0
793.0	38.669	0.05	38.512	38.55	190	0.47	-2.9
904.0	38.261	0.06	38.130	38.15	180	0.50	-3.0

TABLE 5. Bolometric luminosity of SN 1987A from CTIO optical and ESO infrared data U to Q0 data.

Date	$\log_{10}(L_{uvoir})$ (erg s^{-1})	α
(1)	(2)	(3)
13.8	41.293	1.3
14.8	41.309	1.2
19.7	41.371	1.3
24.8	41.438	1.4
25.8	41.449	1.4
30.8	41.504	1.4
32.8	41.525	1.5
33.8	41.536	1.5
34.8	41.544	1.5
35.8	41.556	1.5
36.8	41.569	1.5
37.8	41.584	1.4
39.7	41.607	1.5
42.7	41.640	1.4
43.7	41.653	1.4
44.7	41.668	1.4
46.7	41.688	1.4
47.7	41.699	1.4
58.7	41.796	1.4
59.7	41.805	1.4
68.7	41.861	1.3
73.7	41.880	1.3
74.7	41.885	1.3
79.7	41.899	1.2
80.7	41.901	1.3
98.7	41.867	1.2
101.6	41.844	1.2
103.7	41.829	1.2
104.7	41.812	1.2
106.7	41.787	1.2
108.7	41.755	1.2
110.7	41.722	1.0
111.7	41.706	1.1
115.7	41.630	1.0
122.7	41.544	0.9
132.1	41.501	0.8
157.1	41.390	0.5
158.1	41.389	0.5
159.1	41.381	0.6
164.1	41.361	0.5
195.0	41.230	0.4
198.0	41.214	0.3
201.0	41.202	0.4
260.8	40.950	0.1
273.9	40.894	0.1
280.9	40.869	0.1
293.0	40.812	0.1
308.8	40.744	0.0
316.8	40.712	0.0
348.8	40.576	−0.2
361.8	40.518	−0.3
377.8	40.450	−0.4

1987A. Once these values are set, the next major sources of uncertainty through day 800 are the differences between the photometric datasets employed, differences in the type of interpolation used in the flux integration, and the photometric errors. Through day 813, various combinations of these errors have led to differences of up to 0.03 dex [see Table 5 in Suntzeff *et al.* (1988) and Table 1 in SB for a summary of the errors]. An early (before day 600) systematic difference between the SAAO and ESO/CTIO data in the *I* band led to systematic differences of 0.03 dex. After day 600, when the infrared dominated the flux distribution, this difference disappeared. The difference between the various interpolation schemes yields systematic differences of up to 0.02 dex for all the calculations. To this end, we have chosen a single type of interpolation (linear) and all the data presented here have used this style of integration. We stress that other interpolation schemes will produce systematic differences with the data presented in Tables 3–5.

We estimate that the total error prior to day 600 in any observation is 0.02 dex added in quadrature with the calculated photometric error. The 0.02 dex is meant to be a standard deviation that will crudely reproduce the typical 0.03 dex *range* associated with the systematic differences discussed above. This error is entered in column 3 in Tables 3 and 4. The errors for the bolometric luminosity given in Table 5 are all 0.02 dex or less since the photometric error is smaller than 0.005 dex (see Table 1 in SB). We stress that for the dates before 600, the quoted error is dominated by systematic effects, so relative differences in the bolometric luminosity will generally be much more accurate (<0.01 dex).

For the late time, the photometric and far-infrared extrapolation errors dominate. For days later than 900, the typical error in the bolometric luminosity due purely to photometric errors is 0.02–0.03 dex. This includes the uncertainties in the *U* to *Q*0 magnitudes, the extrapolation from *U* to 3000 Å, but not the extrapolation from 20 μm longwards. The error in the far-infrared extrapolation for days past 600 is larger, but the exact error is hard to quantify because it is an extrapolation. We have attempted to roughly estimate the error in the blackbody extrapolation by fitting, via an interactive program, scaled black bodies of various temperatures and total fluxes to the data. From this series of fits, we estimate an allowed *range* of T_{eff}, total blackbody flux, and flux longwards of 20 μm. We have then added (in quadrature) half the range in the flux longwards of 20 μm to the photometric errors to arrive at the error quoted in column 3 in Tables 3 and 4. A summary of the allowed ranges in bolometric luminosity, T_{eff}, and total flux in the fitted scaled blackbody are given in Table 6.

We have experimented with adding artificial data points at *M* for days 1144 and 1352, to estimate the effect that the

TABLE 6. Uncertainties of the parameters in the bolometric luminosity calculation.

Day	Range in $\log_{10}(L_{uvoir})$ (erg s^{-1})	Range in T_{eff} (K)	Range in $\log_{10}(L_{BB})$ (erg s^{-1})
648	39.23–39.29	290–420	39.00–39.05
670	39.12–39.20	220–350	38.98–39.04
935	38.06–38.20	150–210	37.90–38.05
1055	37.83–38.01	130–180	37.70–37.90
1115	37.54–37.75	140–200	37.50–37.65
1144	37.51–37.71	130–170	37.35–37.60
1352	36.95–37.40	140:–200:	36.65–37.35

missing data has on the bolometric luminosity. Extrapolating the M data to these dates, and adding ± 1 mag to M, changes the bolometric luminosity by less than 0.04 dex, which is much smaller than the errors in the far-infrared extrapolations.

It should be noted that for the late-time bolometric luminosity, the extrapolation into the ultraviolet is beginning to become important. The extrapolation from 3000 to 3600 Å is 3% of the total estimated uvoir luminosity for day 1144. If the flux distribution is flat shortward of 3200 Å the bolometric luminosity could be underestimated by ~ 0.1 dex.

To close this section, we stress once again the rather subjective nature of the fits of a scaled blackbody to the data. For instance, using just the U to Q 0 data on day 648, we find that the possible range in $T_{\rm eff}$ is 290–420 K. This range is greatly reduced by merely adding the one continuum measurement at 100 μm (see Fig. 4 in SB) which restricts the possible $T_{\rm eff}$ to 350–400 K. As the thermal component cools, the fitting procedure, after day 700, relies on just flux points longwards of 5 μm. Since there are only two to four flux points in this region, the fits become more uncertain. It should also be stressed that the *assumption* that a blackbody is an appropriate fit to the far-infrared flux is also a potential source of systematic error. It is possible that the far-infrared fine-structure lines could provide significant cooling in the ejecta nebula. Many of these lines are longward of 20 μm and are not accounted for by the extrapolation. Clearly any measurements in the far infrared and millimeter regions are very important in constraining the late-time behavior of the thermal and line-flux evolution of SN 1987A.

4. DISCUSSION

4.1 Photometric Evolution Through day 600

The interpretation of the broadband magnitude and color evolution of SN 1987A is complicated by the fact that after day 100, the spectrum became dominated by emission lines. Unless the effects of the emission lines are explicitly accounted for, only the general trends of the data in time can be easily interpreted.

In Figs. 2–4, we present the *UBVRI* and broadband color evolution. The general trend of the data through day 400 has been well described previously (see for instance SB, Arnett *et al.* 1990; Hillebrandt & Höfflich 1989). We will give a short summary here. During the first two weeks, the supernova quickly faded as the high temperatures produced by the supernova shock wave cooled to the temperature typical of hydrogen recombination. This produced a much more rapid decline in the U and B colors, where, as can be seen in Fig. 3, $U-B$ reddened by 3.5 mag and $B-V$ by almost 2 mag. The evolution from day 20 to 100 shows a slow rise to maximum at day 90. The evolution during this period was roughly isothermal (the effective temperature declined from 5300 to 4900; see Suntzeff *et al.* 1988), and indeed the optical and infrared colors were quite constant as can be seen in Figs. 3 and 4. This period of evolution has since been modeled as the passage of a diffusion wave of energy produced by the radioactive decay of ^{56}Ni and its daughter products that were mixed into the expanding optically thick nebula. [See the reviews by Arnett *et al.* (1990), and Hillebrandt & Höfflich (1990) for the references on the modeling.] From day 95 to day 125, the supernova declined very rapidly in brightness and reddened suddenly due to the passage of the diffusion wave of energy through the nebular photosphere.

Around day 125, the supernova entered an exponential decline phase. The changeover from the rapid decline from maximum to the exponential decline phase happened in less than one week, and as pointed out in SB, this rapid changeover indicates a remarkable coherence to the nebular emission processes that have not yet been theoretically explained. From day 125 to 300, the broadband colors all declined at exceedingly uniform exponential rates. The actual rates have been shown (Hamuy & Suntzeff 1990) to be a strong function of wavelength, with the colors bluer than V fading more slowly (or even increasing) than the red or near-infrared colors which are close to the 113 day e-folding time which corresponds to the decay rate of ^{56}Co. Although theoretically unexplained, this wavelength dependence is probably an opacity effect in the nebula. The effect of the different exponential decline rates is to make all the colors evolve towards the blue again.

Starting around day 300, the broadband colors began to decline more rapidly at the same time that the gamma rays from SN 1987A began to be important in the energy budget of the supernova. This slight acceleration in the fading of SN 1987A is most obvious in the U light curve in Fig. 2, but all the optical colors began to fade more rapidly at that time.

By day 500, however, the broadband colors began to fade extremely quickly. At the same time, the optical colors shown in Fig. 3 stopped their rapid blueward evolution and began to evolve to the red. The infrared colors also shown in Fig. 4 stopped their blueward evolution and began to evolve rapidly towards the red. In Fig. 5 we present the 10 and 20 μm light curves from the CTIO and ESO data. Starting around day 400, both the 10 and 20 μm fluxes stopped declining and began to brighten. Evidently the flux has shifted from the optical and near infrared to longwards of 5 μm. This behavior has been previously discussed by Suntzeff & Bouchet (1990), and Lucy *et al.* (1989), and is a manifestation of the formation of dust, whose presense was first noted spectroscopically by Danziger *et al.* (1989). This late-time formation of dust around day 300 was actually predicted by Gehrz & Ney (1987) (see also Gehrz & Ney 1990), in analogy to the formation of dust in classical novae.

4.2 Optical and Near Infrared Photometric Evolution After Day 600

Sometime between days 550 and 600, the optical colors experienced their most rapid decline and later began to gradually level off, as first reported by Walker & Suntzeff (1989). This leveling off has continued through the last data point on day 1352. For days 1111–1367, the optical colors were falling with e-folding times in the range 261–352 days. As can be seen in Figs. 2 and 3, *UBVRI* are all falling at roughly the same rate during this period. Over the last 650 days, the supernova has declined by 6.5 magnitudes, yet the differences between the *UBVI* colors have not varied by more than 0.6 mag. (We have excluded R since it is affected by $H\alpha$.)

As discussed by Pinto *et al.* (1988), Woosley *et al.* (1989), and Kumagai *et al.* (1989), other sources of radioactive energy become important in the evolution of SN 1987A past day 1000. The next most important radioactive nuclide is ^{57}Co, which has an e-folding decay rate of 391 days, and is predicted to dominate the bolometric light curve starting around day 1200 (Pinto *et al.* 1988). Soon after-

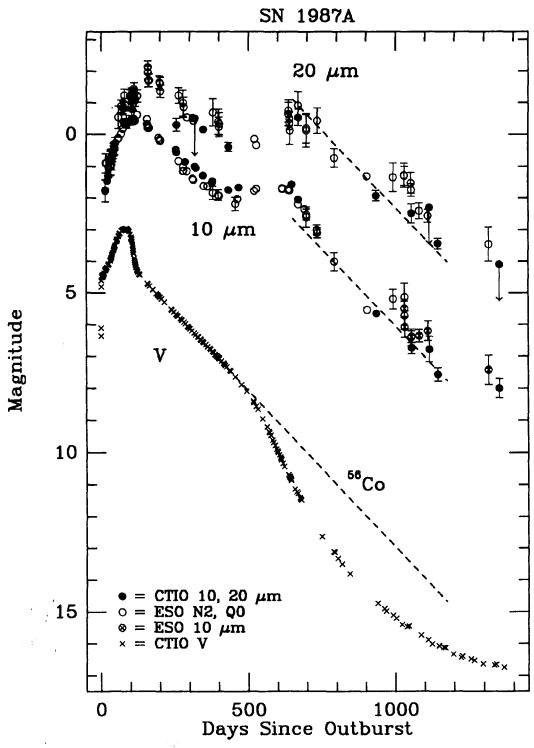

FIG. 5. A comparison of the 10 and 20 μm flux evolution with the V light curve for SN 1987 Å. The ^{56}Co decay law is drawn as a dashed line on the V light curve. Note that the ESO 10 μm magnitudes are either from the narrowband $N2$ filter (open circles) or the broaderband N filter (open circle circumscribing an "×"). The same decay law has been superimposed on the 10 and 20 μm flux data for reference. Note the sudden increase in mid-infrared flux starting around day 450, at the same time the V light began to dim rapidly. The 10 and 20 μm data have been falling at roughly the same rate since day 600. The large, unexplained difference between the ESO and CTIO 10 and 20 μm photometry can be seen at day 1000.

wards, perhaps even by day 1300, ^{44}Ti, which has an e-folding decay rate of 78.2 yr may begin to dominate the energy production. Thus, from these "standard" models, we can conclude that the decline rate after day 1000 is expected to evolve slowly towards an e-folding rate of 391 days or greater.

In Fig. 2, we have sketched in the decay law for ^{57}Co. It is clear that the optical colors are roughly approaching such a rate of decline. Complications such as the unknown wavelength and temporal dependence of the optical opacity, and the possible existence of other energy sources such as ^{44}Ti, or a buried pulsar, preclude a more precise inference to be drawn from the optical data.

The near infrared colors, shown in Fig. 4, after declining rapidly through day 400, have slowly reddened from days 500 to 900. The fact that V (as well as U and B) only reddened modestly relative to the near infrared colors is indicative that dust grains with only a modest wavelength dependence of the scattering cross section (such as few micron-sized particles) must have formed. If very small dust grains formed, a much steeper wavelength dependence, such as that for Rayleigh scattering, would have caused the UBV magnitudes to decline much further. (Alternatively, a very clumpy distribution of the grains would produce a similar behavior.) This can be seen more clearly in Fig. 6 where we plot the V and H light curves. Both colors have faded with the same general rates over 1350 days, even during the time of dust formation around day 600. Comparison of Figs. 4(b) and 6 show that the V and H magnitudes have not changed their relative difference by more than 0.5 ± 0.5 magnitudes from days 20 to 1351, during which time the supernova has faded by over 13 mag!

What is different about the near infrared colors when compared to the optical colors is that around day 900–1000, the reddening has stopped and perhaps begun to evolve to the blue again. The cause of this change in color evolution is not clear, but could be due to the dust becoming optically thin at the infrared wavelengths first.

4.3 Late-Time Evolution of the Ten and Twenty Micron Magnitudes

As shown in Fig. 5, after day 600, the 10 and 20 μm fluxes began to fall with roughly the ^{56}Co decay rate through day 900. A close inspection of the figure reveals that the 10 μm flux actually declined somewhat more rapidly than the 20 μm flux. This is consistent with the thermal source cooling, and indeed, this is exactly what we measured (see column 6 in Tables 3 and 4). The fact that these infrared fluxes are falling at roughly the ^{56}Co decay rate is strong support that the thermal emission is associated with dust that enshrouds the energy source of the nebula, and not due to an infrared echo, which would not be expected to fall at this rate except by coincidence.

The evolution of the mid-infrared fluxes after day 900 is less clear since the ESO and CTIO data differ greatly. In what follows we review and contrast the two datasets.

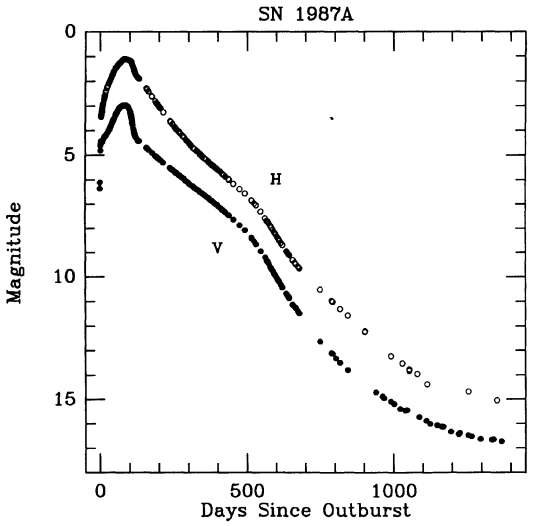

FIG. 6. A comparison of the V and H-band evolution of SN 1987A. Although $V - H$ reddened somewhat around day 500 at the time of dust formation, the general evolution, seen in both colors, has been roughly similar, implying that the scattering cross section for the dust that formed did not have a steep dependence on wavelength.

There are obvious and significant discrepancies with the ESO 10 and 20 μm photometry as shown in Fig. 5. Some of the differences may be due to different filter sets used at the two observatories. The ESO 10 μm photometry through day 1030 (the open circles in Fig. 5) are the $N2$ magnitudes. The $N2$ filter is a narrow filter with $\lambda_c = 9.7$ μm and $\Delta\lambda = 1.4$ μm, where λ_c is the central wavelength and $\Delta\lambda$ is the FWHM of the filter transmission curve. Due to the faintness of the supernova after day 1030, the ESO astronomers changed to a broad 10 μm filter with $\lambda_c = 10.4$ μm and $\Delta\lambda = 5.2$ μm. These magnitudes are shown in Fig. 5 as an open circle with an "×" drawn through the circle. The CTIO 10 μm data were obtained through a single broad filter with $\lambda_c = 10.5$ μm and $\Delta\lambda = 6.1$ μm. The systematic difference in the 10 μm magnitudes of $\sim$0.35 between the CTIO and ESO magnitudes through day 500 could be due to the gross difference in filter characteristics.

The 20 μm filters also are different. The ESO filter has $\lambda_c = 18.6$ μm and $\Delta\lambda = 4.1$ μm, while the CTIO filter has $\lambda_c = 19.6$ μm and $\Delta\lambda = 8.3$ μm. The ESO 20 μm magnitudes are systematically brighter by $\sim$0.6 magnitude through day 500. Although distressing, these differences in mid-infrared magnitudes have very little effect on the estimated uvoir bolometric luminosity. By the time the flux distributions shifts to the mid-infrared around day 600, the CTIO and ESO photometry agree quite well.

Around day 1000, however, discrepancies between the two data sets appear again at both 10 and 20 μm. After day 1000 when the filters used in the 10 μm observations are almost the same, the ESO 10 μm data are apparently systematically brighter than the CTIO data. The 20 μm ESO magnitudes are also systematically brighter. The differences in photometry are particularly extreme for a rather short time period between days 990 and 1055. Since the emission at this time is apparently continuum rather than line emission, and since, in fact, the data a few months later are in closer agreement, some other explanation is required. We have examined the raw ESO and CTIO data, and the data reduction procedures, and find no obvious differences. In particular there are no significant differences in adopted zero-points, individual standard star magnitudes, or observing techniques. The one difference is that the CTIO data were all taken with a 4.3″ beam, while the ESO data were taken with a 5″ aperture. The ESO data *could* be systematically higher if there was a substantial component of extended emission present out to a radius of roughly 2.5″ from the supernova around day 1000, or the ESO data were systematically miscentered with respect to the CTIO data.

This emission would presumably be due to grains heated by the supernova near maximum, such as a light echo (Dwek 1983). We can constrain the models of light echo emission by measuring the emission around the supernova out to 8.8″, based on optical CCD data and infrared imager data. (We have obtained long slit infrared spectra with the CTIO 4 m telescope with IRS, and find that the fuzz, around day 1000, shows negligible nebular line emission. The observed flux in the "fuzz" therefore, must be dominated by scattered light.) We find that for day 1115, the *UBVRIJHK* magnitudes of this emission are (17.0, 16.8, 16.3, 15.2, 15.1, 15.0, 15.5, 15.0) where we have averaged the magnitudes of the *JHK* "fuzz" as given in Table 2. The typical errors on these magnitudes are $\sim$0.3. These magnitudes correspond to a uvoir bolometric luminosity of 36.60 ± 0.10 in units of $\log_{10}$(ergs s^{-1}), which shows that the total emission in scattered light from the surrounding nebulosity is approximately 10% of the supernova's uvoir bolometric luminosity at day 1115. The energy at longer wavelengths must be this amount times the ratio of the dust absorption and scattering cross sections; in order for a significant amount of the ESO/CTIO difference to be due to light echo emission the grain albedo must be 20% or less. If this is the case, then the CTIO data must contain a substantial component of light echo emission as well, and the bolometric luminosity must be significantly less than the value computed from the observations. However, as discussed in SB, since the evolution of the thermal component from days 600 to 900 closely follows the expected energy input from just ^{56}Co, it is unlikely that more than 30% of the uvoir bolometric flux can come from an echo. Thus, we conclude that an echo probably cannot account for the difference between the CTIO and ESO data sets.

The large difference between the two datasets has led to radically different conclusions about the late-time bolometric evolution of SN 1987A (see Bouchet *et al.* 1989b, 1989c; Suntzeff *et al.* 1990a, 1990b), since the flux distribution in the supernova is dominated by these mid-infrared flux points. We have no evidence to doubt either data set at this point, and in the following discussion, we will refer to only the CTIO 10 and 20 μm measurements. We refer the reader to the accompanying paper by the ESO group (Bouchet *et al.* 1991b) for a discussion based on the ESO data.

4.4 The Bolometric Light Curve

In Fig. 7 we plot the estimated uvoir bolometric light curve data as tabulated in Tables 3–5. We have also plotted the *U–M* bolometric light curve given in SB for days 1–500 (but where we have shifted the tabulated *U–M* bolometric points in SB to the linear interpolation values) as a solid line, since the data are so dense. For the symbols that have no

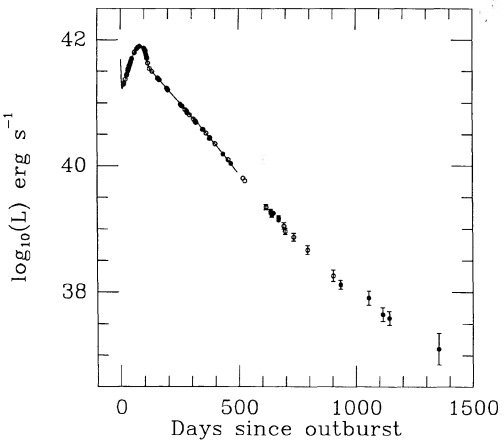

FIG. 7. The bolometric light curve for SN 1987A through day 1352. The solid circles are the CTIO optical and infrared data, and the open circles are the CTIO optical and ESO infrared data as discussed in Suntzeff & Bouchet (1990). The solid line is the *U–M* integration taken from SB. The late-time evolution has an inflection point around day 800 when the bolometric decline lessens.

error bars, the estimated error is smaller than the size of the symbol. The agreement between the CTIO and ESO/CTIO data through day 900 is excellent. A shallow inflection point can be seen in the bolometric decline of SN 1987A around day 800 at which time SN 1987A began to decline at a slower rate.

In Fig. 8 we plot the estimated uvoir bolometric luminosity from the CTIO and the CTIO/ESO data (solid circles), and the late-time luminosities published by Bouchet *et al.* (1991b) (open circles). The brighter 10 and 20 μm mag reported by the ESO group have led to systematically brighter luminosities starting around day 1000 when compared to the CTIO data. We shall not use the ESO data in the fits to the models.

We have compared the observed uvoir bolometric luminosity to the models of the exponential decline of SN 1987A developed by Woosley *et al.* (1989), and Woosley (1990, private communication of the computer source code for the predicted bolometric luminosity). In Fig. 8, we plot the observed data and the model data for three different initial ratios of $^{57}Co/^{56}Co$ with the same initial mass of ^{56}Ni ($0.075\mathcal{M}_\odot$).[3] The three models correspond to "solar", two, and five times the "solar" ratio of $^{57}Co/^{56}Co$, where the "solar" ratio is taken to be the solar ratio of $^{57}Fe/^{56}Fe$ of 0.0243 (Cameron 1982). The initial amount of ^{44}Ti and ^{22}Na are assumed to be $1\times10^{-4}\mathcal{M}_\odot$ and $2\times10^{-6}\mathcal{M}_\odot$, respectively, as predicted by the models discussed by Woosley *et al.* (1989) and Kumagai *et al.* (1989).

Because the luminosity is dominated by the radioactive decay of ^{56}Co from day 125 to 700, the three models differ by less than 0.02 dex. All three models have spectacular agreement through day 700 to the measured uvoir luminosity to within the measurement errors. After day 700, the models show significant deviations as ^{57}Co apparently begins to affect the energy output of the nebula. We find that the best fit model is for five times solar $^{57}Co/^{56}Co$, with extreme ranges of 4–6, through day 1352.

As we will explain later, there is possible reason to believe that, based on the models developed by Woosley & Hoffman (1991) and the late-time x-ray observations of SN 1987A, the initial value of $^{57}Co/^{56}Co$ may be ~ 1.5 solar. If we fix the $^{57}Co/^{56}Co$ ratio at this value, we can explore other sources of energy. In Fig. 9, we present the same curve but with 8 times the amount of ^{44}Ti and 1.5 times solar $^{57}Co/^{56}Co$. We can get adequate fits for ^{44}Ti between 7 and 11 times the standard model value.

Since ^{44}Ti has such a long half-life, making it the dominant late-time energy source is almost equivalent to adding a constant amount of energy to the computed uvoir bolometric light curve. In Fig. 10 we show a model (with the same initial masses of ^{56}Ni, ^{22}Na, and with 1.5 times solar $^{57}Co/^{56}Co$) with a constant energy of 37.3 [in units of $\log_{10}(\text{ergs s}^{-1})$]. Energies within 0.15 dex of this value also can fit the data.

This constant energy source could be a pulsar. The energy is well below the Eddington luminosity for a neutron star of $\sim 2\times10^{38}$ ergs s^{-1}, and is similar to energy inputs expected from pulsars. For instance, the Crab pulsar emits 5.5×10^{36} ergs s^{-1} of pulsed energy (Hasinger 1984; see discussion in Woosley *et al.* 1989). The total energy deposition of the Crab pulsar lies between this value and the energy spin-down rate of the neutron star which is $\sim 5\times10^{38}$ ergs s^{-1} (Coroniti & Kennel 1985). Alternatively, the constant energy input could come from an infrared echo around SN 1987A. As discussed above, optical and infrared images appear to constrain such an echo to the extent that fairly unusual grain properties are required if the echo is to contribute substantially to the observed luminosity.

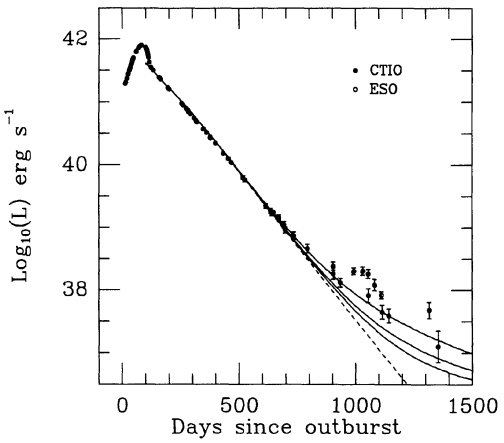

FIG. 8. A comparison of the observed uvoir bolometric luminosity of SN 1987A with model predictions by Woosley *et al.* (1989). The solid lines correspond to 1, 2, and 5 times solar $^{57}Co/^{56}Co$ (see text). The dashed line shows the contribution of ^{56}Co alone. By day 800, additional energy input is needed to fit the observed bolometric luminosity. In particular, five times solar ^{57}Co is consistent with the data. Also plotted as open circles are the late-time value for the bolometric luminosity reported by ESO (Bouchet *et al.* 1991) which are inconsistent with the CTIO data. The ESO data have not been used in the fits.

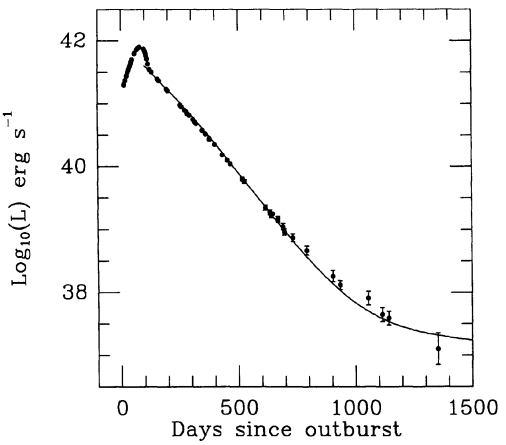

FIG. 9. A comparison of the observed uvoir bolometric luminosity of SN 1987A with model predictions by Woosley *et al.* (1989) for 1.5 times solar ^{57}Co and eight times the predicted amount of ^{44}Ti.

[3]The nuclides produced in the supernova explosion are actually ^{56}Ni and ^{57}Ni which quickly decay to ^{56}Co and ^{57}Co. Thus, when we speak of the "initial" masses of cobalt, we are really speaking of the initial masses of short-lived neutron-rich nickel isotopes. Because we do not see the energy input from the nickel isotopes and because they decay so quickly, it makes more sense to talk of the cobalt isotopes as the "initial" nuclides.

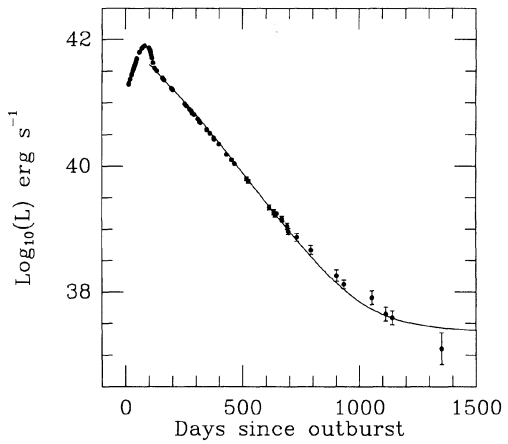

FIG. 10. A comparison of the observed uvoir bolometric luminosity of SN 1987A with model predictions by Woosley *et al.* (1989) for 1.5 times solar ^{57}Co and a constant energy input of 2×10^{37} ergs s^{-1}. This energy input is well below the Eddington luminosity for a neutron star of 2×10^{38} erg s^{-1}.

Both the addition of ^{44}Ti or a constant energy source, while fitting the data, clearly gives an inferior fit to the data compared to the enhanced ^{57}Co model. This is because the data from days 750–900 appear to be too high with respect to the constant energy input models and need an additional 2×10^{38} ergs s^{-1} on day 800 to fit the data. This energy must decay to 2×10^{37} ergs s^{-1} by day 1200 in order to fit the data. All of this is naturally provided by enhanced ^{57}Co.

As our final model fit, we have plotted in Fig. 11 the observed uvoir bolometric luminosity with different assumptions about the extrapolation of the flux longwards of 20 μm. We have also plotted the uncertainty in the estimated bolometric luminosity due to the photometric errors alone. The same three models with 1,2, and 5 times solar ^{57}Co/^{56}Co. In this figure, we plot the data for the assumption that the flux beyond 20 μm follows a Rayleigh–Jeans law with the flux fixed at the observed 20 μm flux point, and for the assumption that there is *no* flux longwards of 20 μm. The assumption of the RJ law extrapolation is consistent with roughly 2.5 times solar ^{57}Co/^{56}Co. The assumption of no flux longwards of 20 μm is clearly too extreme; the flux distribution through day 800 shows that a thermal component must exist, but the comparison with the models is constructive, since it is clear from Fig. 11 that some extra energy source, other than ^{56}Co must be present, even under this extreme assumption. With no flux longwards of 20 μm, the data could be fit by 1.5 times solar ^{57}Co/^{56}Co. Although 5 times solar ^{57}Co/^{56}Co provides the best fit, a more conservative conclusion which includes the uncertainty in the extrapolation, is that the data can be fit with roughly 2.5–6 times solar ^{57}Co/^{56}Co, with 5 times solar being the most likely value.

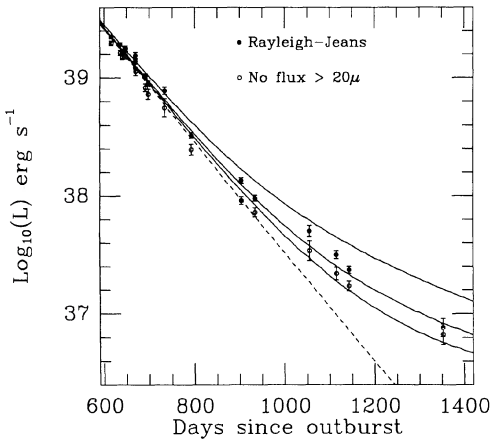

FIG. 11. The calculation of the observed bolometric luminosity of SN 1987A under different assumptions of the extrapolation of the flux longwards of 20 μm. The solid circles refer to a Rayleigh–Jeans law fit to the 20 μm flux, and the open circles refer to the assumption of *no* flux beyond 20 μm. The three curves refer to 1,2, and 5 times solar ^{57}Co/^{56}Co, and the dashed line to the input from ^{56}Co alone. The error bars show the uncertainty in the luminosity from the photometric errors alone. Even under the extreme, and incorrect, assumption that there is no flux beyond 20 μm, it is clear that an additional energy source is needed.

Woosley & Hoffman (1991) have reanalyzed the limits on the amount of radioactive nuclides produced in explosive silicon burning and nuclear statistical equilibrium in light of the estimated bolometric luminosity evolution of SN 1987A presented in this paper. The amount of ^{56}Ni (which quickly decays to ^{56}Co) produced has been set at $0.075\mathcal{M}_{\odot}$, which is the amount needed to reproduce the bolometric evolution from days 125 to 800. Relative to this amount of ^{56}Co, to first order, the production of ^{57}Co and ^{44}Ti can be set by the solar system ratios of ^{57}Fe/^{56}Fe and ^{44}Ca/^{56}Fe. They find that the allowable range of ^{57}Co/^{56}Co lies between one-third and four times solar, with one-half to two times solar being the most likely ratio. They find that the production of ^{44}Ti is more tightly constrained at less than twice solar. We therefore conclude that the observed uvoir bolometric light curve is only barely consistent with the model predictions of ^{57}Co/^{56}Co. The constant energy source of ten times solar ^{44}Ti, modeled in Fig. 9, conflicts strongly with the models discussed by Woosley & Hoffman (1991). *If their model is correct and the blackbody extrapolation is correct, the observed bolometric flux must contain an energy source other than ^{56}Co, ^{57}Co, and ^{44}Ti.*

Support for the lower values of ^{57}Co/^{56}Co predicted by Woosley & Hoffman (1991) comes from infrared spectroscopy and hard x-ray continuum measurements. We discuss the infrared spectral observations first. Danziger *et al.* (1990) concluded from observations of the emission-line flux of the [Co II] 10.52 μm line that the ^{57}Co/^{56}Co must be approximately 1.5 times solar. However, due to significant uncertainties in the observations and the required ionization corrections, the error associated with this estimate is quite large. Varani *et al.* (1990) have attempted to overcome the latter problem by using the [Co II] 1.547 μm and [Fe II] 1.533 μm lines to estimate the cobalt to iron abundance ratio as a function of time. They also conclude that the final ^{57}Fe/^{56}Fe isotope ratio in the ejecta must be 1 to 2 times the solar value. We have replotted the data given in the Varani *et al.* (1990) paper and find that the best fit to the data is actually 2 times solar ^{57}Co/^{56}Co, based on the value for ^{57}Fe/^{56}Fe published by Cameron (1982). We also find that the observations are actually consistent, within the quoted error bars,

with a ratio as large as 3 times solar, and could even be fit by a 4 times solar model if the transition probabilities assumed for one or both of the emission lines were significantly in error. We conclude that the spectral data are not necessarily in conflict with a high $^{57}Co/^{56}Co$ ratio.

The observed hard x rays from SN 1987A have also been used to support a low value of the $^{57}Co/^{56}Co$ ratio. The observations and models are given in the recent work by Sunyaev *et al.* (1990a, 1990b). They have published the hard x-ray fluxes from the HEXE detector of Röntgen observatory aboard the Mir–Kvant module. SN 1987A was observed approximately every 100 days through day 645 in the energy bands 15–45, 45–105, and 105–200 keV. The ^{57}Co decay will produce spectral lines at 122 and 136 keV, which, due to recoil effects, will produce noticeable discontinuities in the x-ray flux at these energies. After day 500, the ^{57}Co density is high enough that these spectral discontinuities should be seen superimposed on the rest of the continuous x-ray flux, which is dominated by the degraded γ-ray emission at 847 and 1238 keV (and higher energy lines) from ^{56}Co. Sunyaev *et al.* (1990b) derive a 3σ upper limit of 1.5 times the solar ratio of $^{57}Co/^{56}Co$, based on three different dates of observations. The individual measurements actually correspond to upper limits of 2.4 (day 580), 3.3 (day 645), and 1.8 (day 830). The latter value is based on a nondetection in all three bandpasses and should be given lower weight. A direct measurement of the 122 keV line in their data leads to an upper limit of six times solar for the $^{57}Co/^{56}Co$ ratio.

Kumagai *et al.* (1989), using the Sunyaev *et al.* (1990b) data, but their own models, come to a different conclusion. They find that the best fit to the hard x-ray data is with a $^{57}Co/^{56}Co$ ratio of twice solar. The actual model that they fit is due to Hashimoto *et al.* (1989) where the predicted $^{57}Co/^{56}Co$ ratio was 2.4 times solar. The error bars in the observed x-ray flux presented by Kumagai *et al.* (1989) in their Fig. 5 for day 600, are consistent with values up to three times solar $^{57}Co/^{56}Co$. While the Kumagai *et al.* (1989) and Sunyaev *et al.* (1990b) estimates for the $^{57}Co/^{56}Co$ ratio are in disagreement due to the different models used, both studies show that there is an upper limit of about three times solar for $^{57}Co/^{56}Co$, with twice solar being more likely.

The observed hard x-ray fluxes and the model predictions seem to be inconsistent with the conclusion that the best fit to the observed uvoir bolometric luminosity has a $^{57}Co/^{56}Co$ ratio of 5 times solar. We end this section by stressing some of the uncertainties in the observations and models. First, more than half of the "observed" flux in the uvoir bolometric flux is actually an extrapolation longwards of 20 μm. As seen in Fig. 11, merely by assuming another form of the extrapolation, we can lower the amount of $^{57}Co/^{56}Co$ needed to fit the data to 2.5 solar. Second, the observed hard x-ray fluxes are right at the threshold of detection, for a source which is so weak that the detected signal is dominated by background events. Small errors in the detector efficiency or background levels can easily affect the detection value. Third, the difference between the predicted hard x-ray fluxes discussed above show that there is also error associated with the choice of the model. Finally, we point out that by day 1000, roughly 75% of the gamma rays are leaking out undegraded. Differences in the average spatial position of the two cobalt isotopes could lead to different optical depths in the gamma ray lines of the different isotopes. This in turn, can lead to different x-ray continuum fluxes than predicted by models where the isotopes are well mixed.

We therefore conclude that, given the errors in the observations and the models, *the observed uvoir bolometric luminosity may be fit with enhanced $^{57}Co/^{56}Co$ of between roughly 2.5 to 4 times solar with no need for additional energy sources,* other than the ^{56}Ni and ^{44}Ti predicted to have formed in the supernova event. However, both the x-ray observations and the models alone may to point towards a $^{57}Co/^{56}Co$ ratio of ~ 2. If we accept that there is only ~ 2 times solar $^{57}Co/^{56}Co$, the observed uvoir flux from SN 1987A with *reasonable* extrapolations longwards of 20 μm implies that there must be another energy source than the predicted radioactive nuclides powering the SN 1987A nebula.

4.5 Optical Spectral Evolution

In Fig. 12 we plot three low-dispersion (17 Å FWHM) optical spectra of SN 1987A obtained with the CTIO 1.5 m telescope between days 953 and 1149. Since the light of stars 2 and 3 could not be excluded from these observations, we have overplotted in the same figure the summed spectrum of stars 2 and 3 obtained at somewhat higher wavelength resolution (10 Å FWHM) and under good seeing conditions with the 4 m telescope on day 1046. An uncontaminated spectrum of the supernova obtained on this same night is shown in Fig. 13. Narrow emission lines due to the circumstellar material originally associated with the progenitor, Sk-69° 202, are readily distinguished from the broader super-

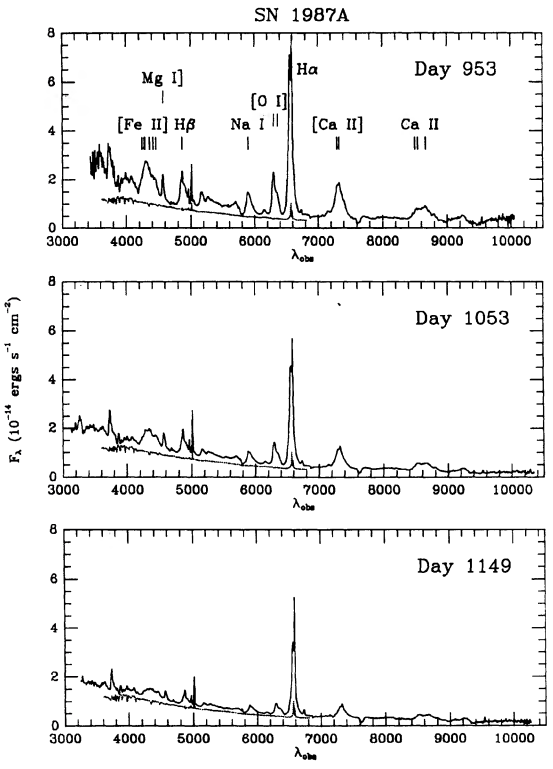

FIG. 12. Low dispersion spectrophotometry of SN 1987A, obtained at the CTIO 1.5 m telescope for days 953, 1053, and 1149. The supernova spectra are contaminated by the light from stars 2 and 3, whose spectra are overplotted to show the level of contamination.

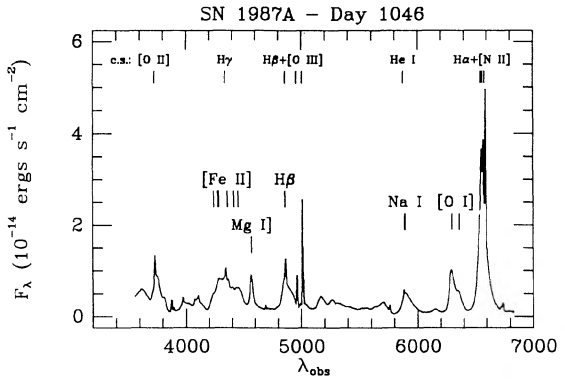

FIG. 13. A higher dispersion spectra of SN 1987A with the contamination of stars 2 and 3 removed.

nova ejecta emission features in the latter spectrum. Note also that there is very little continuum emission due to the supernova itself. As seen in Fig. 12, the relative intensities of the supernova lines have changed remarkably little over the last year. This is also illustrated in Fig. 14, where the observed fluxes of the Hα, [O I] $\lambda\lambda$ 6300, 6364 Å, and Mg I] λ 4571 Å emission lines are shown to have been decreasing at nearly exactly the same rate since day 900. (Note that the Hα fluxes have been approximately corrected for the contribution of the Hα and [N II] $\lambda\lambda$ 6548,6583 Å circumstellar emission lines.) Since the late-time spectra are dominated by emission lines such as these, the equal decline rates seen in the *UBVRI* broadband colors shown in Fig. 2 are likely due to equal decline rates in fluxes of the dominant emission lines. There is no evidence yet in the optical spectra for the emission lines of highly ionized elements such as [O III] $\lambda\lambda$ 4959,5007 Å which might be expected if the dominant

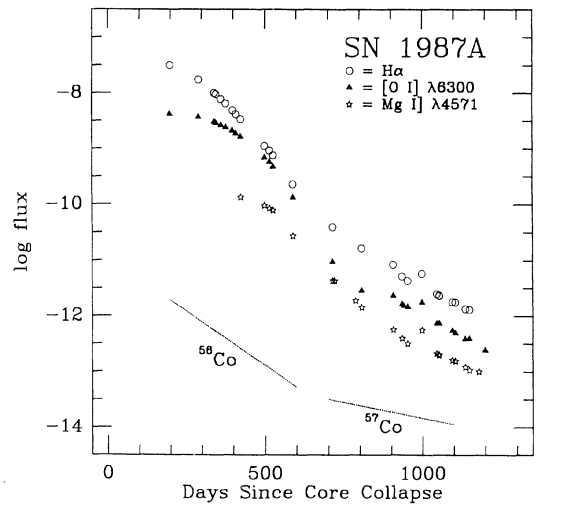

FIG. 14. The evolution of the optical line fluxes for Hα, [O I] λ 6300 Å, and Mg I] λ 4571 Å. The line fluxes began to decline more rapidly than the ^{56}Co decay law starting around day 500, but by day 700, the decline rate has slowed.

energy input source was the high-energy radiation of a pulsar (Fransson 1987).

The optical emission-line luminosities shown in Fig. 14 began to decline more rapidly starting around day 450, but by day 800, the decline had gradually lessened, somewhat reminiscent of the behavior of the optical colors shown in Fig. 2. A sudden drop in the optical emission-line intensities around day 600 was predicted for SN 1987A by Fransson (1987) and Fransson & Chevalier (1987). This so-called "infrared catastrophe" in an Fe-Co plasma was first suggested by Axelrod (1980). The infrared catastrophe occurs when the nebular cooling of the ejecta becomes dominated by the mid- and far-infrared fine-structure lines. However, the evidence for the formation of dust starting around day 450 and continuing through at least day 800 seems unambiguous, since mid-infrared spectra obtained through day 777 show that the flux is predominantly due to continuum rather than lines (e.g., Rank 1990). In addition, the effective size of the blackbody inferred from the effective temperature and infrared flux has expanded with a velocity that is the same as the terminal velocity for the optical emission lines (Suntzeff & Bouchet 1990). The sudden decline in emission-line intensities starting at day 450 can be naturally explained by the extinction produced by this dust.

The fact that we see no dramatic drop in optical line fluxes past day 800 suggests that the "infrared catastrophe" as proposed by Fransson and Chevalier has not yet occurred. However, one could imagine that the supernova nebula is composed of two density states such that small regions of higher density are starting to undergo the "infrared catastrophe," while the rest of the nebula is still cooling slowly. In this case, the optical spectrum would continue to be dominated by the lower density regions and little change would be observed in the relative intensities of the optical emission lines. Some increase in the decline rates of the optical emission line intensities would be expected, but this could be masked by changes in other parameters affecting the line intensities. For example, the decrease expected in the optical line fluxes with respect to the mid- and far-infrared lines could be offset by the possible thinning of the dust. We have argued that the blueward evolution of the optical colors when compared to the near-infrared colors (see Fig. 4) may be evidence that the dust is indeed thinning. If this model were correct, then a significant fraction of the mid-infrared luminosity observed since day 800 would then be due to emission lines rather than dust emission.

Since the dominant fine-structure lines are at 26 μm (Fe II) and 63 μm (O I), we would not have seen the flux from these lines in any of the data presented here (the 26 μm line lies outside the bandpass of our 20 μm filter). Thus, we cannot directly estimate how much of the flux is due to other fine-structure lines participating in the rapid cooling of the supernova nebula. If the 10 and 20 μm bandpasses are dominated by these lines, there should be a large amount of flux in the far-infrared lines, as shown by Fransson & Chevalier (1987). Under this assumption, the far-infrared extrapolation that was used, based on thermal emission, would have to be replaced by model estimates of the far-infrared line fluxes. The flux predicted by such models could conceivably be either less than or greater than the blackbody extrapolation. Unless better fine-structure line fluxes are measured, and models are published appropriate to the observed energy production in SN 1987A for days later than 800, the importance of the "infrared catastrophe" is unknown.

The peak velocities of the Mg I] λ 4571 Å and [O I] λ 6300 Å emission lines are plotted in Fig. 15. These lines were selected for measurement because they are relatively isolated and suffer little or no contamination from the narrow circumstellar shell emission lines. Values obtained through day 805 have been published by Phillips *et al.* (1990). Until day 500, the peak of the Mg I] λ 4571 line (along with the peaks of several other emission lines such as Hα and Na I D) showed a fairly substantial redshift which Witteborn *et al.* (1989) interpreted as arising from electron scattering. However, over this same period, the peak of the [O I] λ 6300 Å line (and the unresolved [Ca II] $\lambda\lambda$ 7291,7324 Å and [C I] $\lambda\lambda$ 9824,9850 Å blends as well) differed in not having a significant redshift. Lucy *et al.* (1990) have noted that most of the lines that showed a redshift are from ions that are very likely to be in close proximity to the ^{56}Co energy source. If the ^{56}Co is distributed in discrete lumps, each of which is surrounded by ionized gas, line photons emitted from within these zones would be more likely to be scattered by free electrons than line photons emitted in the neutral zone.

Between days 550–600, all of the emission line peaks suddenly shifted to negative velocities. This has been cited by Lucy *et al.* (1989) as strong evidence for the formation of dust in the ejecta, although since blueshifts of similar magnitude were observed for emission lines in the near-infrared, an unusual (but not implausible) grain size distribution is implied (Spyromilio *et al.* 1990). Recall that such a "grey" selective absorption was also implied by the similarity of the optical and infrared light curves shown in Figs. 2–4. As Fig. 15 shows, the blueshift of the Mg I] λ 4571 Å line has remained essentially constant since day 700 or so, while that of the [O I] λ 6300 Å peak appears to have reached a maximum value of -750 km s^{-1} around day 1000, and has slowly decreased since to a value of -400 km s^{-1}. If true, the latter observation would suggest that the dust may have started to grow optically thin again. We would emphasize, however, that this result must be taken with caution due to the very low wavelength resolution of the spectra from which the measurements were derived. There are two obvious problems. First of all, high-dispersion observations of the [O I] lines reveal small-scale structure in the profiles which is completely smoothed over in our low-resolution spectra. Second, high-dispersion data show that a weak component of zero-velocity circumstellar [O I] λ 6300 Å emission is actually present which may increasingly affect our peak measurements as the much broader supernova emission fades. We have examined the latter problem by comparing the [O I] λ 6300 Å line profiles in a high-dispersion spectrum of the supernova obtained by R. Stathakis with the Anglo–Australian Telescope on day 1088 (kindly sent to us by Dr. Peter Meikle) and in our own low-resolution spectrum taken nine days earlier. We find the agreement to be quite reasonable considering the difference in wavelength resolution, and conclude that the effect of the circumstellar shell component of emission was probably not significant through this date. However, for later dates our velocity measurements are probably increasing unreliable. If we disregard these, the evidence for a decrease in the blueshift of the [O I] λ 6300 Å peak since day 1000 is only marginally convincing.

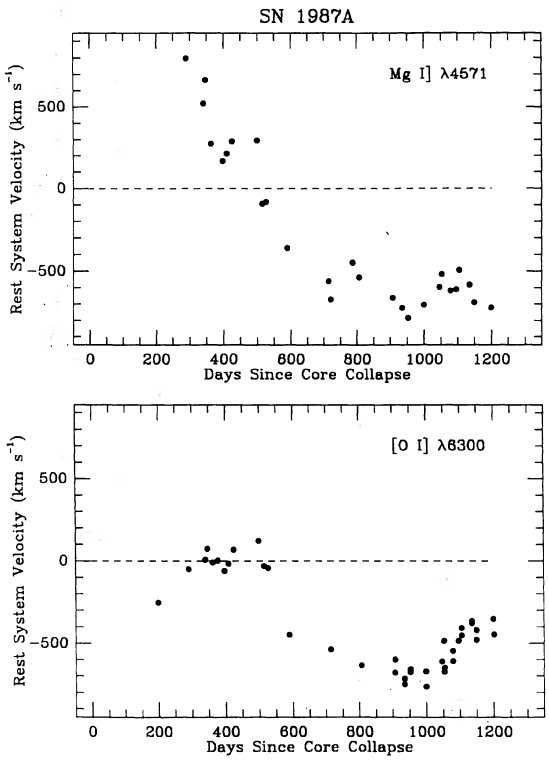

FIG. 15. The temporal evolution of the emission line velocities of Mg I] λ 4571 Å and [O I] λ 6300 Å through day 1200. The velocities underwent a sudden blueshift around day ~450 at the time that dust began to form in the supernova nebula.

5. SUMMARY

We have shown that, starting around day 1000, another source of energy beside the radioactive decay of ^{56}Co is required to explain the temporal evolution of the uvoir bolometric luminosity of SN 1987A. The extra energy seems to be decreasing in time, in that around day 800 roughly 2×10^{38} ergs s^{-1} is needed but by day 1200, only 2×10^{37} ergs s^{-1} is needed. We can obtain an excellent fit to the data assuming that the ^{57}Co/^{56}Co isotope ratio is 5 times the "solar" ratio for ^{57}Fe/^{56}Fe. This result is only barely consistent with the extreme value of 4 times solar permitted by present-day stellar nucleosynthesis theory (Woosley & Hoffman 1991). It is also barely consistent with the fit to the hard x rays around day 600 by Kumagai *et al.* (1989), and is too high for the model fits by Sunyaev *et al.* (1990b). However, the uncertainties in the models, hard x-ray fluxes, and the proposed extrapolation longwards of 20 μm, lead us to believe that a value of 2.5 to 4 times solar ^{57}Co/^{56}Co is consistent with all the data. Alternatively, the observed uvoir bolometric light curve can be fit with a value of 1.5 times solar ^{57}Co/^{56}Co as predicted by the models, and an added energy source that by day 1200, has a luminosity of 3×10^{37} ergs s^{-1}, which is six times the pulsed energy of the Crab pulsar. The model fits in which a constant energy source has been added give fits that are clearly inferior to the models with an enhanced ^{57}Co/^{56}Co ratio.

We wish to acknowledge the cooperation of our colleagues at ESO (P. Bouchet, C. Gouiffes, and J. Danziger) in giving us their infrared data prior to publication and their

openness in discussing details of the sources of differences in the fundamental data and the analysis. We appreciate the extended discussions on the late time evolution of SN 1987A with Stan Woosley. We thank D. Palmer, C. Wheeler, P. Pinto, P. Meikle, G. Varani, and J. Wampler for helpful discussions. We thank D. Terndrup for observing SN 1987A on day 1204 with the CTIO 4 m and InSb imager, and we thank L. Wells and M. Navarrete for their help in observing the supernova with the CCD on the CTIO 0.9 m. We also wish to thank M. Hamuy for obtaining and reducing some of the spectral data presented here. Some of the more difficult references were tracked down by librarians Cathy Van Atta (KPNO) and Sarah Stevens-Rayburn (STScI); we appreciate their help.

REFERENCES

Arnett, W. D., Bahcall, J. N., Kirshner, R. P., and Woosley, S. E. 1989, ARA&A, 27, 629
Axelrod, T. S. 1980, Ph. D. thesis, University of California at Santa Cruz
Bionta, R. M., *et al.* 1987, Phys. Rev. Lett., 58, 1494
Blanco, V. M., *et al.* 1987, ApJ, 320, 589
Bouchet, P., Moneti, A., Slezak, E., le Bertre, T., and Manfroid, J. 1989a, A&AS, 80, 379
Bouchet, P., Danziger, I. J., and Lucy, L. B. 1989b, IAU Circ. No. 4933
Bouchet, P., van Dijsseldonk, Vela, R., and Labrana, F. 1989c, IAU Circ. No. 4839
Bouchet, P., and Danziger, I. J. 1991, A&A (submitted)
Bouchet, P., Phillips, M. M., Suntzeff, N. B., and Gouiffes, C. 1991a, A&A, 245, 490
Bouchet, P., Danziger, I. J., and Lucy, L. B. 1991b, AJ, 102, 1135
Cameron, A. G. W. 1982, in Essays in Nuclear Astrophysics, edited by C. A. Barnes, D. D. Clayton, and D. N. Schramm (Cambridge University Press, Cambridge), p. 23
Catchpole, R. M., *et al.* 1988, MNRAS, 231, 75p
Coroniti, F. V., and Kennel, C. F. 1985, in The Crab Nebula and Related Supernova Remnants, edited by M. C. Kafatos and R. B. C. Henry (Cambridge University Press, Cambridge), p. 25
Danziger, I. J., Gouiffes, C., Bouchet, P., and Lucy, L. B. 1989, IAU Circ. No. 4746
Danziger, I. J., Lucy, L. B., Bouchet, P., and Gouiffes, C. 1990, in Supernovae, Proceedings of the Tenth Santa Cruz Summer Workshop, edited by S. E. Woosley (Springer, Berlin), p. 69
Depoy, D. L., Gregory, B., Elias, J., Montané, A., Perez, G., and Smith, R. M. 1990, PASP, 102, 1433
Dwek, E. 1983, ApJ, 274, 175
Elias, J. H., Frogel, J. A., Matthews, K., and Neugebauer, G. 1982, AJ, 87, 1029
Elias, J. H., Gregory, B., Phillips, M. M., Williams, R. E., Graham, J. R., Meikle, W. P. S., Schwartz, R. D., and Wilking, B. 1988, ApJL, 331, 9
Fowler, A. M., Gillett, F. C., Gregory, B., Joyce, R. R., Probst, R. G., and Smith, R. 1987, in Proceedings of the Workshop on Ground-Based Astronomical Observations with Infrared Array Detectors, edited by C. G. Wynn-Williams and E. E. Becklin (University of Hawaii, Hilo), p. 199
Fransson, C. 1987, in ESO Workshop on the SN 1987A, ESO Conference and Workshop Proc. No. 26, edited by I. J. Danziger (ESO, Garching), p. 467
Fransson, C., and Chevalier, R. A. 1987, ApJL, 322, L15
Gehrz, R. D., and Ney, E. P. 1987, Proc. Natl. Acad. Sci., 84, 6961
Gehrz, R. D., and Ney, E. P. 1990, Proc. Natl. Acad. Sci., 87, 4354
Gouiffes, G., Wampler, E. J., Baade, D., and Wang, L. F. 1989, The Messenger, 58, 11
Hamuy, M. and Suntzeff, N. B. 1990, AJ, 99, 1146
Hamuy, M., Suntzeff, N. B., Bravo, J., and Phillips, M. M. 1990, PASP, 102, 888
Hamuy, M., Suntzeff, N. B., González, R., and Martin, G. 1988, AJ, 95, 63
Hashimoto, M., Nomoto, K., and Shigeyama, T. 1989, A&AL, 210, L5
Hasinger, G. 1984, MPE Report No. 186
Hillebrandt, W., and Höflich, P. 1989, Reports on Progress in Physics, 52, 1421
Hirata, K., *et al.* 1987, Phys. Rev. Lett., 58, 1490
Kumagai, S., Shigeyama, T., Nomoto, K., Itoh, M., Nishimura, J., and Tsuruta, S. 1989, ApJ, 345, 412
Lucy, L. B., Danziger, I. J., Gouiffes, C., and Bouchet, P. 1989, Structure and Dynamics of the Interstellar Medium, IAU Colloquium No. 120, edited by G. Tenorio-Tagle, M. Moles, and J. Melnick (Springer, Berlin), p. 164
Lucy, L. B., Danziger, I. J., Gouiffes, C., and Bouchet, P. 1990, in Supernovae, Proceedings of the Tenth Santa Cruz Summer Workshop, edited by S. E. Woosley (Springer, Berlin), p. 82
Menzies, J. W. 1989, MNRAS, 237, 21p
Phillips, M. M. 1988, in Supernova 1987A in the Large Magellanic Cloud, edited by M. Kafatos and A. G. Michalitsianos (Cambridge University Press, Cambridge), p. 16
Phillips, M. M., and Heathcote, S. R. 1989, PASP, 101, 137
Phillips, M. M., and Williams, R. E. 1990, in Supernovae, Proceedings of the Tenth Santa Cruz Summer Workshop, edited by S. E. Woosley (Springer, Berlin), p. 36
Phillips, M. M., Hamuy, M., Heathcote, S. R., Suntzeff, N. B., and Kirhakos, S. 1990, AJ, 99, 1133
Phillips, M. M., Heathcote, S. R., Hamuy, M., and Navarrate, M. 1988, AJ, 95, 1087
Pinto, P. A., Woosley, S. E., and Ensman, L. A. 1988, ApJL, 331, L101
Rank, D. M. 1990, in ESO/EIPC Workshop on SN 1987A and Other Supernovae, edited by L. B. Lucy, (ESO, Garching) (in press)
Spyromilio, J., Meikle, W. P. S., and Allen, D. A. 1990, MNRAS, 242, 669
Stetson, P. B. 1987, PASP, 99, 191
Suntzeff, N. B., and Bouchet, P. 1990, AJ, 99, 650 (SB)
Suntzeff, N. B., Hamuy, M., Martin, G., Gómez, A., and González, R. 1988, AJ, 96, 1864
Suntzeff, N. B., Phillips, M. M., Elias, J. H., Depoy, D. L., and Walker, A. R. 1990a, IAU Circ. No. 4995
Suntzeff, N. B., Phillips, M. M., Elias, J. H., Depoy, D. L., and Walker, A. R. 1990b, IAU Circ. No. 4996
Sunyaev, R. A., *et al.* 1990a, SvAL, 16, 55
Sunyaev, R. A., *et al.* 1990b, in Supernovae, Proceedings of the Tenth Santa Cruz Summer Workshop, edited by S. E. Woosley (Springer, Berlin) (in press); see also SvAL, 16, 403
Terndrup, D. M., Elias, J. H., Gregory, B., Heathcote, S. R. Phillips, M. M., Suntzeff, N. B., and Williams, R. E. 1988, PASAu, 7, 412
Varani, G.-F., Meikle, W. P. S., Spyromilio, J., and Allen, D. A. 1990, MNRAS, 245, 570
Walker, A. R., and Suntzeff, N. B. 1989, IAU Circ. No. 4881
Walker, A. R., and Suntzeff, N. B. 1990, PASP, 102, 131
Walker, A. R., and Suntzeff, N. B. 1991, in preparation
Whitelock, P. A., *et al.* 1988, MNRAS, 234, 5p
Witteborn, F. C., Bregman, J. D., Wooden, D. H., Pinto, P. A., Rank, D. M., Woosley, S. E., and Cohen, M. 1989, ApJL, 338, L9
Woosley, S. E. 1988, ApJ, 330, 218
Woosley, S. E., and Hoffman, R. 1991, ApJ (in press)
Woosley, S. E. 1990, private communication
Woosley, S. E., Pinto, P. A., and Hartmann, D. 1989, ApJ, 346, 395